EUROPEAN ORGANIZATION FOR NUCLEAR RESEARCH

CERN-EP/87-157
September 1st, 1987

Test of an electromagnetic calorimeter using BaF_2 scintillators and photosensitive wire chambers between 1 and 9 GeV

R. Bouclier [1], G. Charpak [1], W. Gao [1], G. Million [1], P. Miné [1], S. Paul [3],

J.C. Santiard [1], D. Scigocki [1], N. Solomey [1] and M. Suffert [2]

Abstract

We describe an electromagnetic calorimeter constructed from layers of BaF_2 crystals, coupled to low pressure MWPCs with hot TMAE gas as the photosensitive constituent. By making use of the fast component from the BaF_2 scintillation, this detector is well suited for a high rate, intense radiation environment. We present the results of a test performed with our prototype in a 1 to 9 GeV/c beam, which gives an energy resolution better than $4\%/\sqrt{E}$, a position resolution of 1 mm, and a time resolution better than 1 ns. The detector is highly segmented, with tracking capabilities and good e/π rejection. We discuss the possible application to experiments with intense colliders.

Submitted to Nuclear Instrument and Methods.

---

[1] CERN, Geneva, Switzerland
[2] CRN, Strasbourg, France
[3] MPI, Heidelberg, FRG

1. Introduction

The proposition to couple BaF_2 crystals with a MWPC came from Anderson et al. [1] [2] [3] who proposed the name solid state proportional counter (SSPC).

The properties of barium fluoride are the following. It is dense (4.9 g/cm^3), and has a short radiation length (2.05 cm). It is also non hygroscopic, and cheaper than BGO. Its fast ultra−violet component, discovered by Laval et al. [4] has a decay time of 600 ps, and is insensitive to temperature [5] [6]. It has an excellent radiation resistance, more than 10^7 rads ,which has been studied by several authors [7]. [8].

The photons are detected and localized in a low pressure wire chamber. Breskin [9] has extensively studied the properties of such chambers. This device, used to detect the scintillation light of the BaF_2, has the advantages of being cheap, naturally segmented, and not very sensitive to magnetic fields. In order to take advantage of the properties of the SSPC, it is useful to operate the MWPC at low pressure, a few torrs, for two reasons. First, the chambers are then insensitive to the ionization due to the charged particles of the shower, which would introduce large fluctuations in the signal, and spoil the energy resolution. Second, an atmospheric chamber is much slower than a low pressure one; time resolutions less than 1 ns at high energy [11] and 2.4 ns at low energy [12] [13] [14] [15] [16] have already been reported.

The electromagnetic calorimeter prototype, used in the present work, was built and tested at low energies (108 and 200 MeV) in 1984 [17]. After a brief description of the improvements we made, we will report on the experimental procedure used in a PS beam at CERN from 1 to 9 GeV during 1986. We will present results on energy measurement, space resolution and its application to electron/hadron separation. The time resolution and high rate behaviour, which are of extreme importance for future high luminosity hadron colliders, will be studied.

There exist two types of electromagnetic calorimeters: homogeneous and sampling. The best energy resolutions are obtained with homogeneous calorimeters, whereas sampling calorimeters optimize the spatial and angular resolutions, with the lepton−hadron separation. These two families exhibit traditionaly incompatible performances. Our calorimeter can combine the advantages of the two systems.

Concluding with a discussion that summarizes our findings, and a comparison with other experiments using the same technique, we describe alternative designs, concerning crystal size for the imaging properties, or MWPC construction to improve the high rate capability. Some still open problems, like the aging of the chambers and the quantitative effect of the magnetic field are mentionned.

2. The experiment.

2.1 The detector.

The constituents of the detector have been described elsewhere [17] and we briefly mention the main characteristics. It is made of forteen cylindrical barium fluoride crystals, 12.6 cm diameter and 1, 2.5 or 5 cm thick. The total BaF_2 depth is 40.5 cm, which represent 19.3 radiation lengths. Each crystal is preceded by a low pressure MWPC, which detects the BaF_2 scintillation, produced by the development of the electromagnetic shower. Thanks to their low density, the chambers do not interfere with the shower development in the detector, which behaves as an homogoneous calorimeter, despite its segmentation. The longitudinal segmentation was chosen to visualize the shower profile. The whole calorimeter is placed in an 35 liter aluminium tank, containing the gaseous mixture necessary for the MWPC operation.

Each crystal is aluminized on the plane face which is not in contact with the chamber and on the side, for light reflexion (fig. 1). The last plane face is covered with an stainless steel mesh, made of 50 μm diameter wires, spaced by 500 μm. This electrode system was found as efficient as the previous NiCr layer, and easier to make. A voltage of -30 V is applied to this mesh, to repel the photoelectrons liberated in the 3 mm conversion space between the crystal and the first cathode plane. The same voltage is applied to the aluminium plate after the chamber, with separates the crystal from the following MWPC. Each plane is thus optically isolated from the next one.

The MWPC has two cathode planes made of 100 μm diameter wires, orthogonal to each other, to localize in the x and y position, and an anode plane made of 15 μm wires to measure energy and time.

The three planes are separated by 3 mm. The wires are 15 cm long, spaced by 1 mm. The anode is connected to a positive potential. The cathodes are connected to a virtual ground through the amplifiers and their wires are grouped into strips of different widths (0.5 cm for the minimum). The lateral profile of the shower is obtained in x and y, by recording the induced signals on the strips.

2.2 Experimental working conditions.

In the first low energy test, performed with this detector, the experimental configuration was different from the present one. The detector was at room temperature (17 °C). The aluminium tank was first evacuated with a primary and secondary pumping unit. Then a valve, connecting the tank to a bottle containing liquid TMAE, was opened. The TMAE vapour filled all the volume after a few minutes. Due to the low TMAE pressure (0.28 torr at 17 °C), it was necessary to add 3 torrs of isobutane, to have correct working conditions in the MWPC. Then the volume was closed during all the data taking. With this experimental procedure a deterioration of the gain was observed after a few hours. It was necessary to pump and refill with a new gas mixture.

For the work described in this paper, the working conditions were different on two points and as a consequence some modifications had to be made:

1. The detector was heated to optimize the UV photons detection efficiency [6].

2. The gas volume was constantly renewed by a low pressure bubbling system, enabling a continuous operation of the experiment.

Increasing the TMAE vapour pressure, by heating the liquid, decreases the conversion length of the photons. For a given gas depth, the detection efficiency rises. We have measured the pressure curve with a Baratron MKS type 223BHA10. Our data points shown on fig. 2, follow the Clausius – Clapeyron relation as in [18] which is compatible with use at low temperature. In our calorimeter the best temperature was estimated to be 40 °C, for a gas depth of 12 mm. The UV photons mean free path is equal to 5 mm, with a TMAE pressure of 1.4 torr, and the detection efficiency is about 10 photoelec-

trons for 1 MeV lost in the crystal [12] [13] The bottle of liquid was immerged in a water thermostat controled bath regulated to better than one tenth of a degree. To avoid TMAE condensation, the tank was heated to a higher temperature (45 °C) with heating belts wrapped around. The temperature of the gas volume was kept constant within 1.5 °C, by a thermostatic regulation driven by a thermistance placed inside the tank. The detector was also covered with insulating material.

A schematics of the continuous bubbling system is shown on fig. 3. In this configuration, the tank is evacuated once by the primary and secondary pumping units, down to 10^{-5} torr. An isobutane bottle is connected to the TMAE bubbler, kept at 40 °C. The isobutane bubbles through the liquid, carrying away the TMAE vapour to the detector. The other side of the tank has a microleak, or an electric valve driven by a pressure transducer, followed by a refrigerated bath to freeze the TMAE, a charcoal trap and a vacuum pump. By this method the gas volume is continously renewed in the detector. Its pressure is set at 2 torrs (1.4 TMAE and 0.6 isobutane). We have found that adding isobutane is mandatory to ensure an external gas flow to renew TMAE at a sufficient rate (a choice of a gas other than isobutane would probably also be adequate). The pressure transducer was the MKS type 223BHA10 used for the determination of the vapour pressure curve, precise to ± 0.1 torr. With this system we have been able to keep the gain stable within a few percent, as will be explained in detail below, and to operate continuously the apparatus without pumping and filling for three months.

Another improvement was added to the original system: the forteen anodes had separate electrical high voltage connections, since at high energy the signals were strongly different with the longitudinal position in the shower.

2.3 The beam.

Our data was collected in the T7 test beam at the CERN PS. The momentum could be varied from 1 to 9 GeV/c, the $\Delta p/p$ dispersion was 2% (FWHM) and the angular dispersion was 10 mrad. The proportion of secondary particles in the beam was momentum dependant: for the electrons 42% at 3 GeV/c, 20 % at 5 GeV/c and 3% at 9 GeV/c. The end of the data taking had to be done with deutons circulating in the PS. In that case the proportion of electrons was lower: 3% at 5 GeV/c. The burst

length was 0.5 s, during which we usually sent 1500 to 3500 particles in the detector, except for the high rate tests described below.

Figure 4 shows the general environment of our apparatus in the test beam. Upstream were two gas Cerenkov counters C_1 and C_2, for particle identification. The signals from their photomultiplers were recorded by ADCs. Figure 5 shows the correlation between C_2 and the energy measured in the calorimeter.

The Cerenkov counters were followed by two drift chambers Ch_1 and Ch_2 giving the horizontal and vertical position of the incoming particles with a precision of 100μm. They worked at atmospheric pressure with a mixture of 4% methylal, 30% isobutane and 66% argon.

Just in front of the calorimeter were placed three scintillators: P_3 was 20x20 cm^2, P_2 had the same size with a 5 mm diameter hole in the center, P_1 was 2x2 cm^2. P_3 was always part of the trigger, while the signals from P_1 and P_2 were recorded on TDC's in order to select at the analysis stage the events well centered in the detector.

Downstream of the calorimeter, a one metre long iron block stopped all the particles except muons. It was followed by two 20x20 cm^2 scintillators μ_1 and μ_2 , used for tagging muon events.

Two types of data were taken: muons for calibration, electrons (with a controlled percentage of pions). The muon trigger was a coincidence of $P_3.\mu_1.\mu_2$ and the electron trigger was $P_3.P_1.C_1$. It was also possible to rotate the calorimeter at 90 degrees and take data on vertical cosmic rays with a special two counter trigger. This set−up was used to monitor the gain stability over long periods, when the beam was off.

2.4 The acquisition electronics.

Our apparatus included 256 electronic channels for the cathodes and 14 for the anodes. For the cathodes we used the same amplifiers and line receivers as in [17] the only modification being an attenuator, by a factor of 60, to handle higher energies. Each line was recorded on one ADC. The dispersion on the gains was $\pm$10%, and the sensitivity was 400 mV/pC.

The 14 anode channels were improved to handle high rates up to 250 khz and to enable timing measurements. Each channel consisted of a charge amplifier, located on the detector, followed by a 6 dB attenuator on some lines. Then the signal was split into two directions. The first one was shaped and fed into a constant fraction discriminator (Ortec 934) before going to a TDC. The second one was shaped for charge measurement, then fed into an attenuator box and finally into the ADC. Two attenuations were possible, corresponding to two types of data collection, muons or electrons. The attenuation values had to be different because the electrons deposited more energy than the muons. Also each chamber plane, relative to the others, had different amounts of energy deposited. We could compensate for the gain differences, and the longitudinal shape of the electron shower. Table 1 gives the different values of the resistors, attenuations and crystal thickness for all the planes. The method to determine these values will be described in the section dealing with calibration.

The total length of the signal in the MWPC was about 3 μs, including the drift of positive ions. We used a 600 ns gate on the ADCs, which was enough to include the maximum of the signal. The data acquisition was performed with a CAMAC system connected to a PDP 11/24 from Digital Equipment Corp. The behaviour of the anode channels at rates up to 250 kHz was tested with a random pulser: no significant shift was measured in the ADCs data. We found an equivalent noise between 100 keV and 2 MeV on the forteen channels, the average being equal to 700 keV.

3. Energy measurements.

3.1 Calibration.

As mentionned in section 2.2, each plane of the calorimeter had its own high voltage power supply. We adjusted the voltages so that there were no ADC overflows on the cathode channels during a 5 GeV/c data collection run with electrons. Their range was distributed between 305 and 330 V, corresponding to a gain of the low pressure MWPC close to $4x10^3$. Then we determined the values of the attenuators for the anode channels, which were different for electron and muon runs (table 1), to get a

reasonable signal in the ADCs. When the beam momentum was higher than 5 GeV/c, all the forteen high voltages were lowered by 10 V, in order to decrease the gain by a factor of two.

The muon signal was very clean, even for the thinnest 1 cm crystal, as can be seen in figure 6 showing the histogram of the pulse height of one muon, leaving a 6.5 MeV ionization energy. The disymmetry coming from the Landau distribution is visible. For this reason all the energy resolutions were measured in full width half maximum (FWHM), and then converted into variance. Here we find a value $\sigma(E)/E = 28\%$. This energy resolution is good enough to use the position of the muon peak p_i in each crystal to calibrate the calorimeter. The energy given in the plane i by an electron E_i can be calculated, knowing the crystal width L_i, the attenuation factors for the electrons A^i_e and for the muons A^i_μ, by to the equation:

$$E_i = 6.5\, L_i\, A^i_e\, ADC_i / A^i_\mu\, p_i$$

where ADC_i is the electron signal measured by the ADC connected to plane i. The total energy deposited in the calorimeter by an electron shower is simply the sum of the forteen E_i calculated by this method. The procedure is correct only if the response for muons and electrons is the same. It is known that this assumption is not true in sampling calorimeters [19] due to transition effects. However our apparatus is, in fact, an homogeneous calorimeter, since the MWPC are almost transparent to the shower, and is expected not to suffer from such a problem. This point will be discussed in section 3.3.

The operating mode for taking data was the following: each electron run at any energy was preceded and followed by a muon run at 5 GeV/c, with the same high voltages, for the purpose of calibration and to check the gain stability. Several thousand events were recorded, giving a statistical error on the gain $\approx 0.5\%$. The main error came from the uncertainty on the determination of the peak position p_i, equal to the width of one ADC channel. It is estimated to be $1\% \pm 0.5\%$.

3.2 Gain stability.

Monitoring the gain, and trying to keep it as stable as possible, is extremely important for a detector aiming at an energy resolution of the order of a few percent. A qualitative check was made during long periods with cosmic rays, the calorimeter being in vertical position. We tested the continuous flowing

system developed for this experiment, and could maintain the apparatus in working order for several months, without any pumping or cleaning.

During the beam periods we collected muon calibration runs with 5000 events each. The fluctuations of the peaks for the forteen crystals are shown in figure 7, as a function of the time. They stay within a few percent, and no general shift is detectable in 34 hours.

A more precise determination was performed with a 120000 events data collection lasting 12 hours with 5 GeV/c electrons. The results are shown in figure 8, each point is the energy peak for the whole calorimeter, calculated with 1000 events. The precision is much better than the other measurements since the energy resolution is $\sigma(E)/E = 1.7\%$ for 5 GeV/c electrons; we can then observe short time fluctuations. One can see a modulation with a period of 20 minutes and an amplitude of the order of 2%. There exists an other phenomenon having the same period in our setup: the heating cycle of the gas tank. This temperature was not as well regulated as the one of the liquid TMAE bottle. Also, for technical reasons the heat source was located around the aluminium cylinder and had to diffuse into the gas, where was located the thermistance which drove the thermostatic loop. Probably the temperature fluctuations of a few degrees produce modifications of the pressure and outgassing through the walls of the calorimeter, which are impossible to control. To minimize this effect in future devices, it would be useful to heat from inside and to control the temperature in and out of the tank, reducing the duration of each heating cycle.

3.3 Energy resolution and linearity.

In the previous measurement [17] with 108 MeV and 200 MeV electrons the energy resolution was $\sigma(E)/E = 12.7\%$ and 8.5% respectively. In the experiment described in this paper a measure in the same region of energy was performed with minimum ionizing muons, which deposit 263 MeV in the 40.5 cm total depth of BaF_2. We obtain 10.6% (figure 9). Figure 10 shows the energy spectrum given by 9 GeV/c particles. One can distinguish clearly the peak of minimum ionizing particles (π and μ), interacting pions giving a wide spectrum and the electron peak centered near 8 GeV, with a $\sigma(E)/E = 1.7\%$. A portion of the shower energy ($\approx$ 1 GeV) leaked because of the finite size of the detector. A

simulation using the EGS [21] program predicted a loss of 982 MeV through the sides of the calorimeter, and 82 MeV at the back. Thus the longitudinal leaks are negligible (less than 1%) for every energy of our test; on the contrary the lateral leaks are very important. They were calculated by EGS, and the result displayed on figure 11 shows that they are around $11-12\%$, for incoming energies greater than 500 MeV. All the results presented in the following will be corrected for this effect.

The linearity of the calorimeter between 1 and 9 GeV is indicated in figure 12. This picture demonstrates the perfect linearity of the apparatus in our energy range and as a consequence the linearity of the fast component of BaF_2. Measurements of the good linearity of a barium fluoride calorimeter have been reported between 2 and 40 GeV [20] for the slow component detected by silicon photodiodes. Our muon data at 263 MeV are also plotted and fit correctly with the straight line of electrons. This confirms the assumption that muons and electrons give the same response.

Table 2 gives the measured energy resolution for different energies. It indicates the contribution coming from leaks, calculated by EGS, and the contribution from the beam momentum spread. The two last lines give the corrected resolution with its uncertainty. These results are summarized in figure 13, the curve represents an energy dependance $\sigma(E)/E = 3.9\% / \sqrt{E}$. This determination was made after a cut in the total energy spectrum, to remove the electrons from the hadrons and muons. Additional cuts using the Cerenkov counters or the centered events traversing the 5 mm hole in P_2, did not improve significantly the resolution.

Let us estimate some effects which contribute to the energy resolution. Some are energy independant, as for example the calibration, giving 1%, but most of them decrease with energy. The photoelectron statistics is an important factor since the quantum efficiency of the BaF_2-TMAE coupling is small ($\approx$ 10 photoelectrons / MeV). Its contribution is estimated as:

$$\sigma(E)/E = \alpha / \sqrt{E}$$

where:

$$\alpha = \sqrt{(\sigma_p/p)^2 + (\sigma_g/g)^2}$$

following reference [11] ; p is the mean number of photoelecrons per GeV ($\approx$ 10000) and g is the average gain in the chambers. The first factor follows a Gaussian law: $\sigma_p^2 = p$. The second one is due to the gain fluctuations in the chambers and is estimated to be the same order as the first one then:

$$\alpha = \sqrt{2/p} \quad \text{and} \quad \sigma(E)/E = 1.5\% / \sqrt{E} \ \text{(GeV)}$$

Let us now estimate the contribution coming from the direct ionization by the shower particles traversing the low pressure MWPC. As far as we know, no measurement exists of the total ionization in an isobutane−TMAE gas mixture. But this data is well known for pure isobutane: 195 ion pairs per centimetre and atmosphere [22]. The number of ion pairs n_s produced by the crystal scintillation is derived from the measured quantum efficiency (10 photoelectrons / MeV), and the dE/dx (6.5 MeV per cm of BaF_2). For a 1 cm crystal we expect n_s = 65 ion pairs in the 12 mm sensitive depth of the MWPC. If we assume a total ionization equal to n_i = 1 ion pair in the same volume, for 1.4 torr of TMAE added to 0.6 torr of isobutane, we finally get the ratio:

$$R = n_i/n_s = 1/65 = 1.5\text{x}10^{-2}$$

This is an upper limit of the "pollution" from direct ionization because the crystals are 1, 2.5 or 5 cm. The typical resolution of a sampling calorimeter, with MWPCs measuring the shower by ionization is $20\%/\sqrt{E}$ (GeV). Then the contribution of ionization to the total resolution is:

$\sigma_i = 0.2\ R\ /\ \sqrt{E}$ or

$\sigma_i = 0.003\ /\ \sqrt{E}$ which is much lower than the measured $3.9\%\ /\ \sqrt{E}$.

The electronic noise was found on average to equal 700 keV, and its contribution is negligible for energies higher than 1 GeV (less than $0.1\%/\sqrt{E}$). We estimated the gain fluctuations at a level of 2% and this contributes to a small amount: $2\%/\sqrt{12} = 0.6\%$.

If we add quadratically the five contributions discussed above, we find for 1 GeV a value $\sigma(E) = 2\%$. The difference with the experimental data may be caused by non estimated contributions, like for example some non uniformity between the center and the edge of crystals.

4. Position measurements.

4.1 Position resolution.

The two drift chambers Ch_1 and Ch_2 measured the horizontal and vertical position of incoming particle, respectively X_1 , X_2 , Y_1 , Y_2 , with a precision of 100μm. D represents the distance between the

two drift chambers, and L the distance between Ch_2 and the average maximum of the electronic shower. One can deduce the lateral coordinates of the center of the shower, taking into account the angle of each beam particle by the formula:

$$X = X_2 + (X_2 + X_1)\, L / D$$

$$Y = Y_2 + (Y_2 + Y_1)\, L / D$$

The angular spread of the beam was momentum dependant. It was not negligible at 1 GeV/c, but was almost zero for higher momenta. In that case we took simply $X = X_2$ and $Y = Y_2$.

In each MWPC plane we calculated the centre of gravity of the cathode signals to get the position of the shower centre X_i , Y_i . Their was insufficient data to calculate an individual calibration for each cathode strip, but we checked a posteriori the absence of large fluctuations by the linearity of the position measurement and by the regularity of the lateral profiles (next paragraph). Then we determined the X_c and Y_c coordinates mesured by the calorimeter by the formulas:

$$X_c = \Sigma\, (X_i/\sigma x_i^2) \,/\, \Sigma\, (1/\sigma x_i^2)$$

$$Y_c = \Sigma\, (Y_i/\sigma y_i^2) \,/\, \Sigma\, (1/\sigma y_i^2)$$

where σx_i (σy_i) were the resolutions measured in the plane i for the x (y) coordinate. These weigths were chosen so as to minimize the final error in X_c and Y_c. Figure 14 shows the correlation between X_2 and X_c for electrons at 9 GeV/c. We can observe a good linearity in a range of a few cm, indicating that the relative gains exhibit no troublesome fluctuation. Figure 15 is a plot of the resolution distribution $X - X_c$, at the same energy; its FWHM is equal to 2.5 mm. Figure 16 summarizes the results from 1 to 9 GeV, plotted in standard deviation, together with a curve $\sigma = 3.6 / \sqrt{E}$ (mm/GeV). The resolution does not follow precisely this parametrization; it decreases from 3.5 mm at low energy, but saturates at 1 mm after 5 GeV.

4.2 Imaging the shower development.

The forteen planes segmentation of the apparatus enables an easy visualization of the longitudinal shower development, as in a sampling calorimeter. Moreover the detection by the MWPCs gives information on the lateral development and on the position. Figure 17 shows a simulation by EGS of a 9 GeV electromagnetic shower where only the electrons and positrons are represented.

Figures 18 a and b show the relative longitudinal energy distribution for 1 and 9 GeV showers. We find a good agreement between the simulation and the data.

The lateral profiles measured by the cathode strips are given in figure 19 plane by plane (the last two planes are omitted since they were not segmented). These plots were used to monitor the relative calibration of the gains in the transvere direction: two planes had dead channels which were removed from all calculations. In the first two crystals, 1 cm thick, the energy loss is almost identical at 1 and 9 GeV because the electrons interact on the average after one radiation length. The effect on the incoming energy becomes visible after these layers. The comparison with the profiles of 7 GeV/c muon events (figure 20) gives a idea of the imaging possibilities of this technique.

The separation capability for two showers simultaneously present in the detector (for example two photons from a π^0) can be evaluated by the width in the first planes. It is equal to $\approx$ 1 cm (FWHM) in the first two planes and $\approx$ 2 cm in planes 3 and 4. In fact the separation is probably better since these numbers include the beam width (1 cm at 9 GeV/c) and divergency.

4.3 Hadron versus electron rejection.

In an electromagnetic calorimeter the main source of hadronic background is the interaction π^- p $\rightarrow$ π^0 n (or π^+ n $\rightarrow$ π^0 p), which can simulate an electronic shower in the detector. These events can be rejected by two methods:

a) If the detector has a good energy resolution and if the incident particle energy is known, a cut on this variable can reject the hadrons with a good precison.

b) If the detector is well segmented longitudinally and laterally, the position of the interaction and the shape of the shower can be used to discriminate electrons and hadrons. In BaF_2 the radiation length is X_0 = 2.05 cm and the nuclear interaction length is λ = 50 cm. Of course a better rejection factor is obtained by combination of these two methods.

To study this problem we started with a data sample of 140000 events at a momentum of 5 GeV/c. A clean sample of 2549 pions was extracted by a cut on the first Cerenkov counter signal, on which we applied criteria a) and b).

a) A first energy cut consisted in the elimination of the events for which the measured energy E_m represented less than 70% of the peak energy of the electrons E_e: $E_m < 0.7\ E_e$. This cut eliminated 0.7% of the electrons and left us with 10 pion candidates which could simulate electrons out of the 2549. After a cut on the second Cerenkov counter C_2 , to correct for C_1 inefficiency, the remaining numbers were respectively 7 and 2480. Thus the value of the rejection factor is:

$$r_{e/\pi} = 7 / 2480 = 2.8\ 10^{-3}$$

This energy cut was rather loose. With a sharper selection, for example $E_m < 0.85\ E_e$, 2% of the electrons were eliminated, but only 6 candidates remained. After a cut on C_2 we were left with 3 candidates out of 2480, and the new rejection factor was:

$$r_{e/\pi} = 3 / 2480 = 1.2\ 10^{-3}$$

b) For the second cut, we used only the longitudinal information to discriminate pions and electrons. The lateral development used in some analysis [19] would certainly improve the result, but needs a detailed simulation and was jeopardized by the limited diameter of our detector.

b1) In a simplified analysis we considered three parts in the calorimeter. The first included the four crystals at the beginning, where the electrons deposit a fraction of their energy not very far from minimum ionizing particles. In the second part, made by crystals 5 to 8, the shower exhibits the highest energy deposition, whereas the pions have still a low interaction probability. The third part consisted in the last five thick crystals where most of the pion interactions take place, but where only the tail of the electromagnetic shower is seen. In that last section it is generally difficult to distinguish between a pion and an electron. Let us define the ratio R_c of the energy deposited in the second part, over the total energy seen in the calorimeter. The value of R_c was calculated for each event of the pion sample defined above and for a clean electron sample (39761 events) selected by a cut on C_1 signal. In figure 21a, the percentage of eliminated electrons is given by the proportion of events at the left of the cut, 10.6%. The pions simulating electrons are at the right of the cut on the figure 21b. Their number is 9.7%, which gives a rejection factor $r_{e/\pi}$ equal to $9.7\ 10^{-2}$. Taking into account the second Cerenkov counter did not change this data. We tested other partitions of the detector into three sections: they all gave a worse result.

b2) In another method, still based on the shape of the shower ignoring spectrometric information, we used the complete forteen plane segmentation. For each event we compared the signal E_i in each chamber (i = 1 to 14), to the average signal for minimum ionizing particles $<E_\mu>_i$. If $E_i < k <E_\mu>_i$, where k is a parameter to adjust, the particle was considered to be minimum ionizing and was rejected as a candidate to simulate an electron. In the reverse case, we assumed that the particle interacted. This method, not only eliminates minimum ionizing particles, but also determines the interaction plane. The electrons interact in the beginning of the calorimeter (90% in the first three crystals), whereas the pions interact along the whole length. Since the interaction point was known for each event, the rejection factor was simply obtained by dividing the number of pion events of this type in the first crystals, which could simulate electrons, by the total number in the pion sample.

Table 3 summarizes the results obtained for $2 < k < 8$, with a cut on the first two planes (1 X_0) and on the first three planes (2.5 X_0). It gives the percentage of pions eliminated by the minimum ionizing criterium the rejection factor $r_{e/\pi}$ and the percentage of rejected electrons. One can see that the cut on the first two planes gives a good rejection factor, but at the expense of a high percentage of rejected electrons. The best compromise is reached with a cut on the three first planes and k between 4 and 6. For example, with $k = 5$, one gets $r_{e/\pi} = 5.4\ 10^{-2}$ and 2.8% loss of electrons. An additional cut on the second Cerenkov counter did not change this result.

It is clear that the best rejection factor can be obtained by using simultaneously the two methods a) and b), when the incoming energy is measured. For example the association of a) and b1), with an energy cut $E_m < 70\%$, eliminated 3 pions out of 7. The result is:

$$r_{e/\pi} = 4 / 2480 = 1.6\ 10^{-3}$$

After an energy cut $E_m < 85\%\ E_e$, no event remained. We can give the following upper limit, with a 90% confidence level:

$$r_{e/\pi} < 2.3 / 2480 = 9\ 10^{-4}$$

5. Time measurements.

5.1 Time resolution.

We measured the time resolution with electron data at 5 GeV/c, on the anode channels. The best result was obtained by averaging planes 4 and 5, which corresponds to the position of the maximum deposition of energy by an electromagnetic shower. The mean was calculated with weights inversely proportional to the variance, to minimize the final error.

The main component of this resolution is the jitter coming from the fluctuation of the materialization position of the UV photons in the detector. If we neutralize the drift space by reversing the voltage (+ 30 V), we keep only the electrons produced in the MWPC. Thus the time resolution is improved, but the energy resolution is degraded, because a factor of 7 is lost in the signal height.

We measured the time resolution in the two configurations:

1. with the drift space

2. without the drift space

Figures 22a and b show the results obtained in the two cases: 1.5 ± 0.1 ns and 1.3 ± 0.1 ns (FWHM). After the substraction of the jitter due to the trigger counter P_3, equal to 1.2 ns FWHM, we are left with the following results, expressed in standard deviation:

1. $\sigma_1 = 400 \pm 200$ ps

2. $\sigma_2 = 170 \pm 130$ ps

5.2 High rate capability.

An important feature for an apparatus, foreseen to operate in high intensity beams, is the ability to work at high rates. Three parameters have to be considered in this problem:

1. The occupation time, defined as the duration of the physical signal caused by one particle traversing the detector.

2. The integration time, determined by the electronics as the time the gate is opened to measure the signal.

3. The timing resolution, which is the precision of the determination of the impact of the particle.

Our prototype was tested at 5 GeV/c with a counting rate, measured by P_3, varying from 6 kHz to 800 kHz. With the experimental working conditions described in sections 2.2 and 2.4, we had the following values for the three parameters:

1. The occupation time was equal to the drift time of the positive ions in the MWPC, i. e. 3 μs.

2. The integration time was chosen to be 600 ns, to completely include all of the signal from the electrons.

3. The time resolution was better than 600 ps, as shown in the previous section.

The first parameter comes from a physical process, intrinsic to gaseous detectors. The maximum theoretical rate that the chambers can handle at a given spot without a modification of their properties is consequently $3x10^5$ events per second, in a continuous flux. Beyond this value the accumulation of positive ions between the electrodes decreases the gain. The quantitative effect is affected by the actual signal processing, like differentiation. It has to be measured and compared to the expected resolution and linearity in energy. In fact the practical capability depends of the segmentation of the detector. The quoted number corresponds to a maximum rate per module. In our prototype, where only the forteen anode channels were equipped with adequate high rate electronics, one module is a 15x15 cm^2 MWPC. For a detector segmented in strips having the size of an electromagnetic shower, say 3 cm, this number would be multiplied by a factor of 5. The best configuration would be to make all measurements using rectangular pads 3x3 cm^2, for which the limit is 8.5 MHz.

The second parameter gives a theoretical limit equal to 1.5×10^6 events per second. If two events are separated by less than 600 ns, there appears a pile−up effect which caused a dispersion of the measured signals in the ADCs. As before the effect depends of the segmentation of the calorimeter. The quoted rates concern an ideal case where the events are regularly spaced in time. One should also take into account the Poisson statistics and the arrival of the beam particles in bunches.

For the third parameter, it is clearly not a limitation at high rate since it is several orders of magnitude smaller than the two others.

Our experimental study consisted in the relative measurement of the gain for electrons and muons on the forteen anode planes, as a function of the counting rate. The beam had a mixture of electrons, hadrons and muons in variable proportion, depending upon the momentum, which was measured with the Cerenkov counters. The important cause of variation being the space charge effect in the MWPCs, the relevant parameter to characterize the rate is then the average energy deposited in the calorimeter per event. This number varied with the nature of the particles circulating in the PS (protons or deutons). For deutons it was equal to 0.4 GeV, and for protons 1.1 GeV. Figure 23 gives the result as a function of the number of "minions" per seconds (equivalent minimum ionizing particles). Two measurements were made using electrons, with drift space and without drift space. Detection of minimum ionizing muons was not possible without the drift space, because the signal was small. The space charge effect is expected to be more pronounced in the drift space, where it competes with a field lower than in the MWPC.

Figure 23 demonstrates that without the drift space one can tolerate higher counting rates without a substancial loss in gain. In fact, in that configuration, the amount of signal is decreased by a factor of 7 in the MWPC, the photons which materialized in the 3 mm of drift space went undetected. It is interesting to plot the same gain measurement as a function of the intensity per wire unit of length. This is done in figure 24. This intensity I is calculated for each chamber plane by the formula:

$$I = Q\, E_{dep} / A\, N\, E_e$$

where E_{dep} is the energy deposited in the calorimeter per second, E_e is the beam energy (5 GeV), N is the number of wires per unit of length in a MWPC and A is the area of a shower estimated from EGS and the measured profiles (2800 mm^2 on average). The charge Q is defined by:

$$Q = ADC\ Att\ Npc / G$$

where ADC stands for the ADC output of that plane, Att for the attenuator value, Npc for the number of picocoulombs per channel (= 0.25) and G for the electronic gain (= 256). The error on I comes essentially from the estimation of A. For the value I we use the average on the forteen planes of the calorimeter, the signals being roughly equalized after the tuning of the attenuators and the MWPC high voltages. Figure 24 shows that the gain decline begins around 10^{-10} A/mm and reaches 25% for I $\approx 10^{-9}$ A/mm in the configuration a). The common range for a) and b) is too narrow to conclude for a real discrepancy between the behaviours in the two conditions.

6. Discussion.

6.1 Specific properties of this calorimeter.

The tests performed between 1 and 9 GeV/c with this prototype calorimeter demonstrate that the low pressure continuous bubbling ($\approx$ 2 torr) and the precise temperature controls (40°C and 45°C) improve the ease of operation. Continuous working over long periods is now possible with high stability for the MWPC gain, comparable to the precision in energy.

The energy resolution $3.9\%/\sqrt{E}$ is of the same order as the performance of a good homogeneous calorimeter, lead glass for example. The result found by the authors of reference [10] [11] who used a single BaF_2 crystal to measure minimum ionizing particles, is in agreement with ours: they find $3.5\%/\sqrt{E}$ for a deposition of 67.8 MeV. Our longitudinal segmentation of forteen crystals has probably deteriorated the energy resolution, but gives the possibility to achieve a position resolution and an electron/hadron separation comparable to specialized sampling calorimeters.

The position resolution obtained is equal to 3.1 mm at 1 GeV/c and 1.2 mm at 9 GeV/c. The e/π rejection is $\approx 5 \times 10^{-2}$ at 5GeV/c, without using the energy information. The lateral shape of the shower was unused in our rather simple analysis. It is known [19] that the addition of this information improves the rejection by a factor of 3 to 5. Higher energies are also expected to be more favourable, both for the position resolution and for the electron/hadron separation. For this last point one order of

magnitude has been quoted at 100 GeV. This type of calorimeter should reach an e/π rejection factor of the order of 10^{-3} for energies higher than 100 GeV. The good energy resolution, combined with a good rejection factor, which can be obtained without magnetic field, makes this device particularly attractive for the TeV region. We have demonstrated in another study [13] that crystals as small as 5x5 mm^2 area can be used efficiently to detect low energy nuclear sources. We think than the imaging capability of the calorimeter can even be improved by a choice of small parallelepipeds instead of large cylindrical monocrystals, as discussed in section 4.4.

The timing resolution is better than 600 ps, and can reach 300 ps when the drift space is neutralized. Woody et al. [11] find the same effect: their best result (800 ps FWHM) is obtained with negative bias, ie. without drift space in our notation. The improvement of the timing by the suppression of the drift space is paid for by a loss in detected light and consequently a deterioration of the energy resolution. One can imagine another configuration, in which the MWPC is directly in contact with the crystal. The vapour pressure of TMAE can be increased by heating at 55°C , to get a mean free path of the photons $\approx$ 2.5 mm. The probalility of photoelectric conversion in the chamber alone is then 90%, equal to the value at 40°C in the present configuration. However the energy resolution is probably worse since the electron collection mechanism is different. In the actual geometry most of the electrons are produced in the drift space and they are amplified identically by the MWPC. In the other design all of the electrons would be produced in the chamber, where the gain varies with the position. Those produced near the anode wires are less amplified. This effect, which exists certainly at a low level with the present design, would introduce fluctuations in the energy measurement and would be the cause of a deterioration in energy resolution.

6.2 The high rate problem.

As pointed out in the section 5.2, the high rate capability of a detector increases with its segmentation. For an electromagnetic calorimeter it is useless to go further than the size of the electromagnetic shower.

The gain loss ($\approx$ 25% at 10^{-9} A/mm) could probably be minimized by suppressing the drift space, although our measurement (fig. 20) is not conclusive. We would then choose the configuration without the drift space, which gives the best resolution in time, at the expense of the energy resolution.

The experimental working conditions were chosen to have the highest gain in the MWPCs. The high voltage was set in each plane so that low energy depositions could be seen in the cathode strips. Attenuators were used for the anode signal for both muon and electron data collection. Another method, more delicate, could be to operate with different voltages for calibration and for normal data taking, without attenuators. It is clear that limiting the gain of the chambers could decrease the space charge effect by one order of magnitude and optimize the detector for high rates.

An improvement in electronics would probably improve the high rate behaviour. Higher sensitivity amplifiers would allow a lower gain in the chambers. They would also, with a more adapted shaping of the signal, allow a shorter gate for the ADCs compared to the 600 ns we used. A proportional reduction of the pile−up would be expected.

6.3 Some other problems.

The behaviour of an electromagnetic calorimeter in a strong magnetic field is an important property, since this type of detector is often placed close to the magnet in a colliding beam experiment. Recent measurements [23] exhibit a decrease in the gain of a SSPC in fields of a few kG, especially when the magnetic field is perpendicular to the drift electric field of the MWPC. The origin of this effect, and its influence on the properties of the calorimeter certainly deserves a special study. The first planned application of a SSPC is a highly efficient veto counter working inside a magnet, for the AGS experiment 787, [11] designed to detect very rare kaon decays.

The exceptional radiation resistance of barium fluoride would be a little advantage if the wire chambers used to detect the light were destroyed by large fluxes of particles. The aging due to polymerisation is well known at atmospheric pressure, the maximum tolerated charge per unit length of a wire is on the order of 0.1 to 1 C/cm. Recent tests [24] made with TMAE and methane or isobutane give the very pessimistic limit of 10^{-4} C/cm. At low pressure the situation may be different, and traces of additives

in the gas or in the material of the MWPC can change dramatically the result. We have not seen any measurable effect in our studies but we were far below the quoted numbers. For the moment this question is unsolved.

In addition to the scintillation light, there is some Cerenkov light which is produced by relativistic particles crossing the BaF_2 crystals. A simple evaluation shows that, taking account of the shorter wavelength of these UV photons and of the maximum sensitivity of TMAE at 150 nm, the numbers of photelectrons produced by the two effects should be of the same order. An application of using this Cherenkov effect in gamma ray astronomy was proposed [25]. Yet the refractive index of BaF_2 is 1.56 and the Cerenkov angle equal to 38° is bigger than the limiting angle of 37° . In principle Cerenkov photons emitted by particles running parallelly to the axis of the crystals are trapped, in contrast with the scintillation photons emitted isotropically. Multiple scattering in the electromagnetic shower may change this result and it is possible than some proportion of the light we measured was in fact due to the Cerenkov effect. A high sensitivity to this additional source of signal would probably be disturbing since it can introduce non linearities and a variation of the efficiency with the angle, etc. An increase in light is not needed since we already have a lot of photons from the high energy shower. In any case a study of this effect by shooting beam particles at various angles through an SSPC, would be useful.

6.4 Calorimetry for future accelerators.

The calorimeters which will be used in future experiments on very high luminosity accelerators SSC or LHC have to satisfy a list of requirements, which we now discuss, following ref. [26].

1. The speed of the detector is a crucial parameter if the expected luminosity is 10^{33} $cm^{-2}\sigma-1$ with 10^8 interations per second. The delay between bunches is $\approx$ 15 ns. Our time resolution, σ < 300 ps, gives the possibility to distinguish events from different bunch crossings. It can even disentangle events coming from the same bunch crossing, within a one nanosecond window, which otherwise would be superimposed.

2. The energy resolution is important, not only for single particles, but also for jets and missing tranverse momentum. The search for the Higgs boson, and new particles in the range of a few hundred GeV/c^2, requires a jet$-$jet mass resolution of a few percent. Our actual detector is as performant as most homogeneous electromagnetic calorimeters in this respect.

3. The granularity of a calorimeter was initially requested for the identification of the electrons close to the jets. The quoted number for the angular separation, from the interaction point, is $\Delta\phi \approx 0.03$. We can have a very fine granularity with BaF_2 since long rods, with a 5x5 mm^2 area, are feasible and have been tested [13] at low energy.

4. The absolute calibration must be kept and monitored within 1%. We have shown how to calibrate our detector by muons with a precision of 1%. The stability was of the order of 2% but it could be improved by a thermostatic system more precise that what we had during the test ($\pm$ 1.5°C).

5. The uniformity of the detector must be better than 1% so that it does not dominate the energy resolution at high energy. In a BaF_2 calorimeter this parameter is dependent of the variation of the amount of light emitted by each crystals and of mechanical tolerances on the MWPCs.

6. A high density is required for compacity and the length of the calorimeter must be long enough to contain most of the electromagnetic shower. Although BaF_2 is the most dense inorganic scintillator after BGO, its density is not at the requested level ($>$ 8 g/cm^3). A total crystal length of 40 cm represents 22 radiation lengths, and it does not include the thickness of the read out MWPCs. One possible solution is to separate the calorimeter into two parts. The first one, 10 to 15 X_0 long, would be homogeneous, as the actual prototype. It will contain 95% of the energy of the showers below 10 GeV and have the highest energy resolution. The second part would be a sampling calorimeter made from BaF_2, MWPCs and lead sheets. It will measure the tail of the high energetic showers.In this region the energy resolution is anyhow dominated by the crystal homogeneity and calibration, and can suffer a reduction of the

light output. With this design it is possible to obtain a higher compacity, without disturbing too much the energy resolution.

7. In consideration of the high luminosity of the accelerator it is mandatory for any detector to accept radiation doses up to 10^6 rads. BaF_2 is for the moment the only dense scintillator which stands such values. However the behaviour of the low pressure MWPCs in these extreme conditions has to be investigated.

8. A good linearity for events up to 5 TeV is an useful property for any calorimeter. We have tested from 0.2 to 9 GeV, and another group [20] has tested, with a different readout scheme, to 40 GeV. No deviation from linearity was found for BaF_2.

9. A good hermiticity, ie. a minimum of dead regions in the calorimeter, is an important parameter for the detection of missing neutrinos. In a of BaF_2 calorimeter the crystals, being non hygroscopic, can be closely packed. No cryostat is needed in this technique and the dead space is due mainly to the passway of the cables for the MWPCs.

10. A good e/π separation based on the pattern in a calorimeter, can only be obtained by using both the longitudinal and lateral measures of the shower. Our simple analysis has shown the very good imaging capability of the detector and a reasonable expectation to reach $\approx 10^{-3}$ at 100 GeV.

7. Conclusion.

We have investigated the performances of an electromagnetic calorimeter consisting of BaF_2 scintillators and wire chambers at a temperature of 40 °C. It is possible to operate continuously this device for several months at low pressure, as soon as the TMAE is renewed by a constant flowing gas system. Minimum ionizing particles are very clearly seen, with an energy resolution of $\sigma(E)/E = 10.6\%$. They are used for calibration and gain monitoring. A precise measurement of the gain fluctuations with the

electrons shows an amplitude of 2%, the limiting parameter being probably our present thermostat regulation.

We find an energy resolution for electromagnetic radiation equal to $3.9\%/\sqrt{(E)}$ and calculate that it is mandatory to operate at low pressure, to avoid a degradation of this number by direct ionization of the gas in the MWPCs.

The position resolution for an electron shower, derived from the center of gravity method, is 3.5 mm at 1 GeV and 1 mm at energies higher than 5 GeV. The e/π rejection at 5 GeV/c is $5.4\ 10^{-2}$, without using the incident energy information, and better than $9\ 10^{-4}$ when this information is used. Better performances are certainly feasible after a more refined analysis and taking into account the transverse shape. The technique enables a very good segmentation both longitudinal and lateral. Thus it combines the advantage of sampling calorimeters (imaging capability) with the characteristics of homogeneous ones (good energy resolution, homogeneity).

The time resolution we measured is better than 600 ps. With different working conditions we can obtain better than 300 ps, but the energy resolution is then degraded. A test of the calorimeter in a high intensity beam showed that the gain begins to decline by 25% for a rate of $4x10^6$ minions per second, or 10^{-9} A/mm of wire. This rather good performance can probably be ameliorated by suppression of the drift space and an upgrading of the electronics.

Clearly some questions are unsolved: behaviour in magnetic field, aging of the chambers due to time or irradiation, influence of Cerenkov effect. However a critical comparison of the characteristics of this technique, with the requirements of detectors for future colliders, shows already that the SSPC is a very good candidate for electromagnetic calorimetry.

References

[1] D. F. Anderson, Phys. Lett. B118 (1982) 230

[2] D. F. Anderson, R. Bouclier, G. Charpak and S. Majewski, Nucl. Instrum. Methods 217 (1983) 217

[3] D. F. Anderson, G. Charpak, Ch. von Gagern and S. Majewski, Nucl. Instrum. Methods 225 (1984) 8

[4] M. Laval, M. Moszynski, R. Allemand, E. Cormoreche, P. Guinet, R. Odru and J. Vacher, Nucl. Instrum. Methods 206 (1983) 169

[5] P. Schotanus, C.W.E. van Eijk, R.W. Hollander and J. Pijpelink, Nucl. Instrum. Methods A238 (1985) 564

[6] M. Suffert and G. Charpak, CERN – EP internal report 86 – 03

[7] S. Majewski and D. Anderson, Nucl. Instrum. Methods A241 (1985) 76

[8] A. J. Caffrey et al., IEEE Trans. Nucl. Sci. NS – 33 (1986) 230

[9] A. Breskin, Nucl. Instrum. Methods 196 (1982) 11

[10] C. L. Woody, C. I. Petridou and G. C. Smith IEEE trans. Nucl. Sci. 33 (1986) 136

[11] C. L. Woody, BNL experiment 787 technical note no. 120 (1986)

[12] P. Miné et al., IEEE Trans. Nucl. Sci. NS – 34 (1987) 458

[13] P. Miné et al., Symposium on Wire Chambers in Medical Imaging, Corsendonk, Belgium, June 28 – 30 1987

[14] D. Scigocki. Thesis, Université de Savoie, 1987

[15] P. Schotanus, C.W.E. van Eijk, R.W. Hollander and J. Pijpelink, Nucl. Instrum. Methods A252 (1986) 255

[16] P. Schotanus, C.W.E. van Eijk, R.W. Hollander and J. Pijpelink, IEEE Trans. Nucl. Sci. NS – 34 (1987) 272

[17] D. F. Anderson, G. Charpak, W. Kusmierz, P. Pavlopoulos and M. Suffert, Nucl. Instrum. Methods 228 (1984) 33

[18] D. F. Anderson, IEEE Trans. Nucl. Sci. NS – 28 (1981) 842

[19] C. W. Fabjan, Calorimetry in high energy Physics, Techniques and concepts in high−energy physics, Ed. T. Ferbel, Plenum Publishing Corporation 1985

[20] E. Lorenz, G. Mageras and H. Vogel, Nucl. Instrum. Meth. A249 (1986) 235

[21] W. R. Nelson et al., SLAC−265 (1985)

[22] F. Sauli, CERN−EP internal report 77−09

[23] C. L. Woody and D. F. Anderson, Fermilab−pub 87/42

[24] J. Va'vra, IEEE Trans. Nucl. Sci. NS−34 (1987) 486

[25] I. Giomataris and G. Charpak, Wide angle high energy gamma ray Cherenkov telescope with good energy resolution, submitted to International Union of Pure and Applied Physics 20th International Cosmic Ray Conference, 2−15 August 1987, Moscow, USSR.

[26] Report on the task force on detector R & D for the SSC. LBL SSC−SR 1021

FIGURE CAPTIONS.

1. Schematics of the calorimeter and details of one MWPC.

2. TMAE vapour pressure as a function of the inverse of the absolute temperature in degrees Celsius, including points from [17].

3. Schematics of the gas continuous flowing system.

4. Setup of our experiment in the test beam.

5. Correlation between pulse height in Cerenkov counter C_2 and the energy measured in the calorimeter, for a 3 GeV/c beam.

6. Pulse height delivered in a 1 cm thick crystal by minimum ionizing muons, corresponding to an energy equal to 6.5 MeV.

7. Relative variation with time of the mean pulse height measured for muons in each of the forteen crystals.

8. Relative variation with time of the mean pulse height measured for 5 GeV/c electrons in the calorimeter.

9. Energy spectrum for muons depositing 263 MeV in the calorimeter.

10. Energy spectrum measured for 9 GeV/c incident particles in the calorimeter.

11. Proportion of the energy of an electron shower lost by side leakage in our detector, simulated by the EGS program.

12. Linearity response of the calorimeter for electrons energies ranging from 1 to 9 GeV, corrected for side leakage. Minimum ionizing muons are also plotted.

13. Energy resolution as a function of the incoming energy.

14. Correlation between the position of a 9 GeV electron measured by a drift chamber in the beam and by the center of gravity of the shower in the calorimeter.

15. Difference between the positions of a 9 GeV electron measured by a drift chamber and by the calorimeter.

16. Position resolution as a function of the incoming energy.

17. Simulation of a 9 GeV electromagnetic shower in the calorimeter, displaying electron and positron tracks.

18. Relative longitudinal energy distributions for 1 and 9 GeV showers.

19. Lateral energy distribution for 1 and 9 GeV/c electrons

20. Lateral energy distribution for 7 GeV/c muons.

21. Distribution of R_c , the ratio of the energy deposited in the center of the detector, over the total energy seen, for 5 GeV/c electrons (top) and pions (bottom).

22. Time spectra with drift space (top) and without (bottom).

23. Relative gain as a function of the number of minimum ionizing particles per second.

24. Relative gain as a function of the intensity per unit of length in the wires of the MWPCs. point end

Plane No.	Resistances		Attenuation	
	R_μ (kΩ)	R_e (kΩ)	Att_μ	Att_e
1	0	1.96	1	20.6
2	0.3	1.96	4	20.6
3	0.1	3.83	2	39.3
4	0.1	3.83	2	39.3
5	0.1	3.83	2	39.3
6	0.1	3.83	2	39.3
7	0.1	3.83	2	39.3
8	0.1	3.83	2	39.3
9	0.1	3.83	2	39.3
10	0.3	3.83	4	39.3
11	0.3	3.83	4	39.3
12	0.3	3.83	4	39.3
13	0.681	1.96	7.81	20.6
14	0.3	1.96	4	20.6

Table 1

E (GeV)	0.108	0.2	1	2	3	5	7	9
$(\sigma_E/E)_{meas}$ (%)	12.7	8.5	6.1	3.5	2.7	1.7	1.7	1.5
$(\sigma'_E/E)_{leak}$ (%)	5.9	4.7	2.03	1.44	1.62	0.97	0.82	0.72
$(\sigma_E/E)_{beam}$ (%)	0	0	0.85	0.85	0.85	0.85	0.85	0.85
$(\sigma_E/E)_{corr}$ (%)	11.2	7.1	5.7	3.1	2.4	1.1	1.5	1.0

Table 2

k	2	3	4	5	6	7	8
Min. ioniz. pions (%)	37.2	57.6	66.9	69.7	71.4	72.6	74.1
$r_{e/\pi}$ (cut on first two planes) (%)	13	6.2	4.2	3.3	2.6	2.4	2
Rejected electrons (%)	6	15.5	25.3	36.5	46	56.4	64
$r_{e/\pi}$ (cut on first three planes) (%)	19.5	9.3	6.6	5.4	4.8	4.4	4.1
Rejected electrons (%)	0.2	0.6	1.3	2.8	4.6	7	10

Table 3

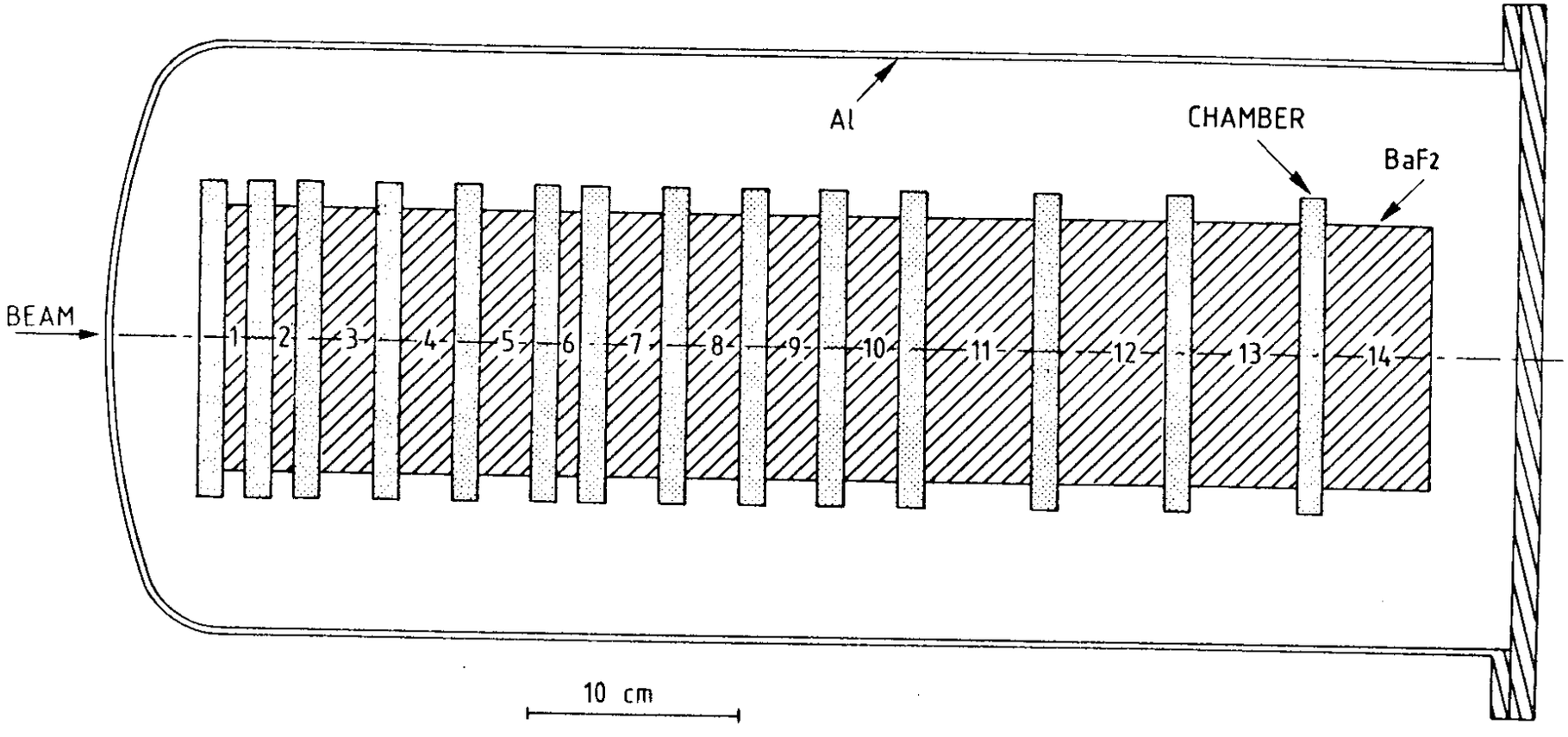

Figure 1a

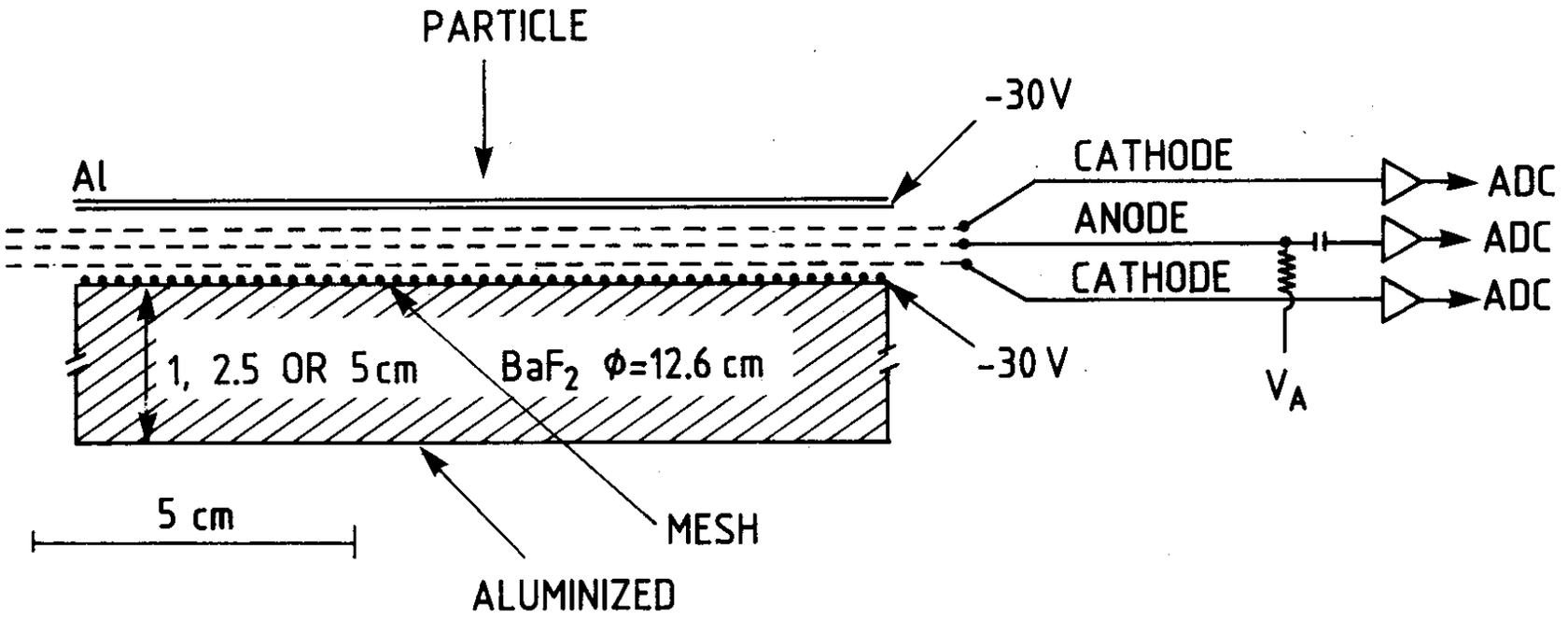
PARTICLE
-30V
Al
CATHODE
ANODE
CATHODE
ADC
ADC
ADC
1, 2.5 OR 5cm
BaF2 φ=12.6 cm
-30 V
VA
5 cm
MESH
ALUMINIZED

Figure 1b

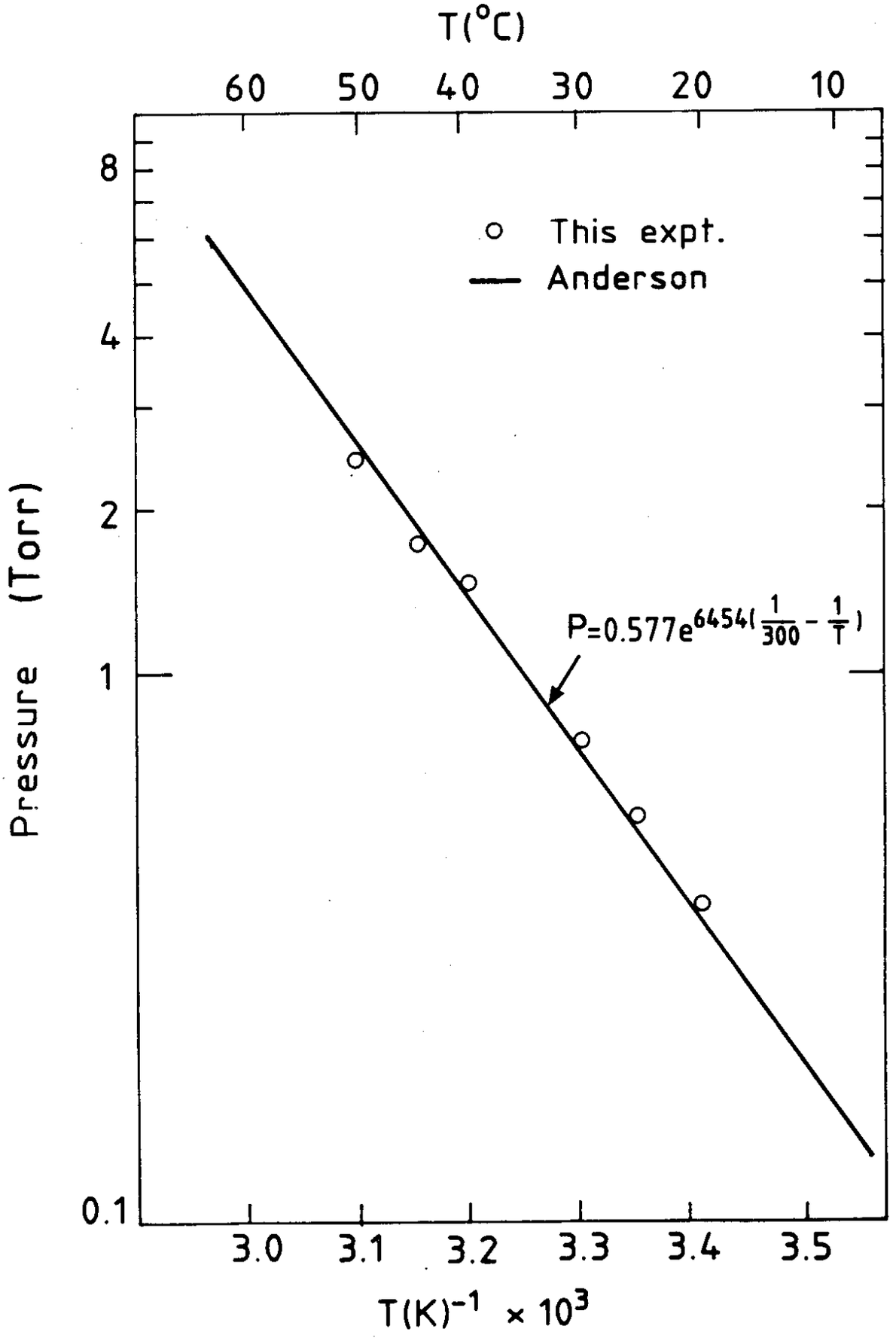
T(°C)
60
50
40
30
20
10
8
4
2
1
0.1
Pressure (Torr)
This expt.
Anderson
P=0.577e^{6454(1/300 - 1/T)}
3.0
3.1
3.2
3.3
3.4
3.5
T(K)^{-1} × 10^3

Figure 2

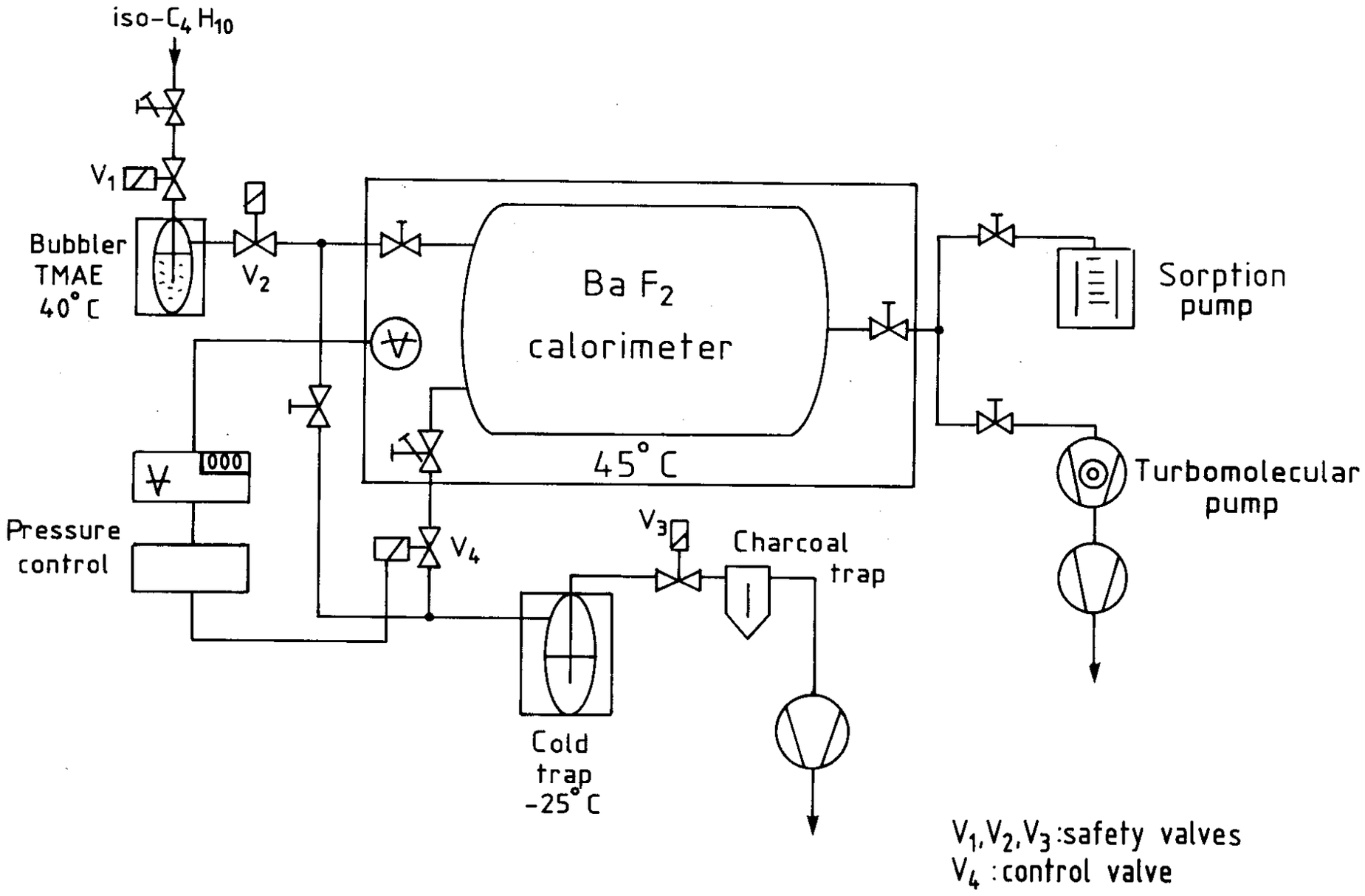
iso-C_4H_{10}
V_1
Bubbler
TMAE
40°C
V_2
Ba F_2
calorimeter
45°C
Sorption
pump
Turbomolecular
pump
Pressure
control
V_4
V_3
Charcoal
trap
Cold
trap
-25°C
V_1, V_2, V_3 :safety valves
V_4 : control valve

Figure 3

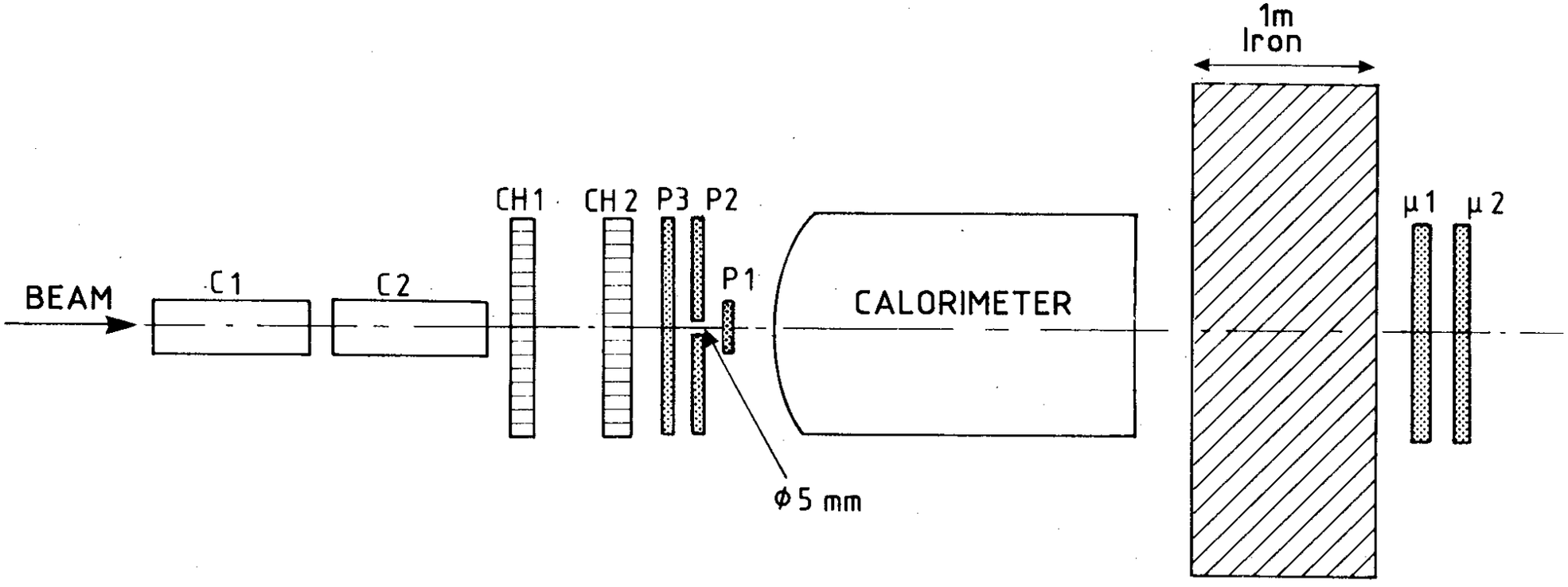

Figure 4

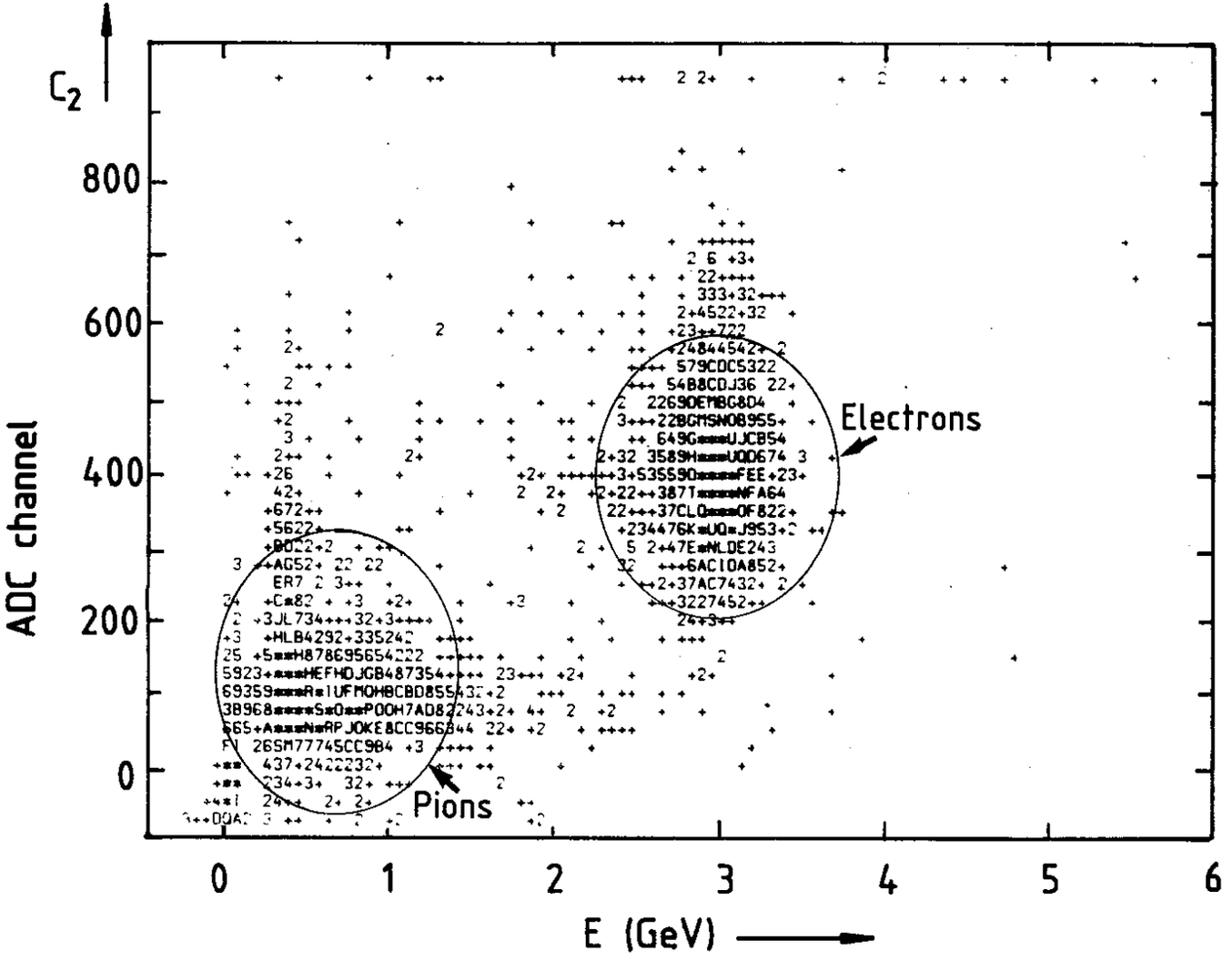
C2
ADC channel
800
600
400
200
0
0
1
2
3
4
5
6
E (GeV)
Electrons
Pions

Figure 5

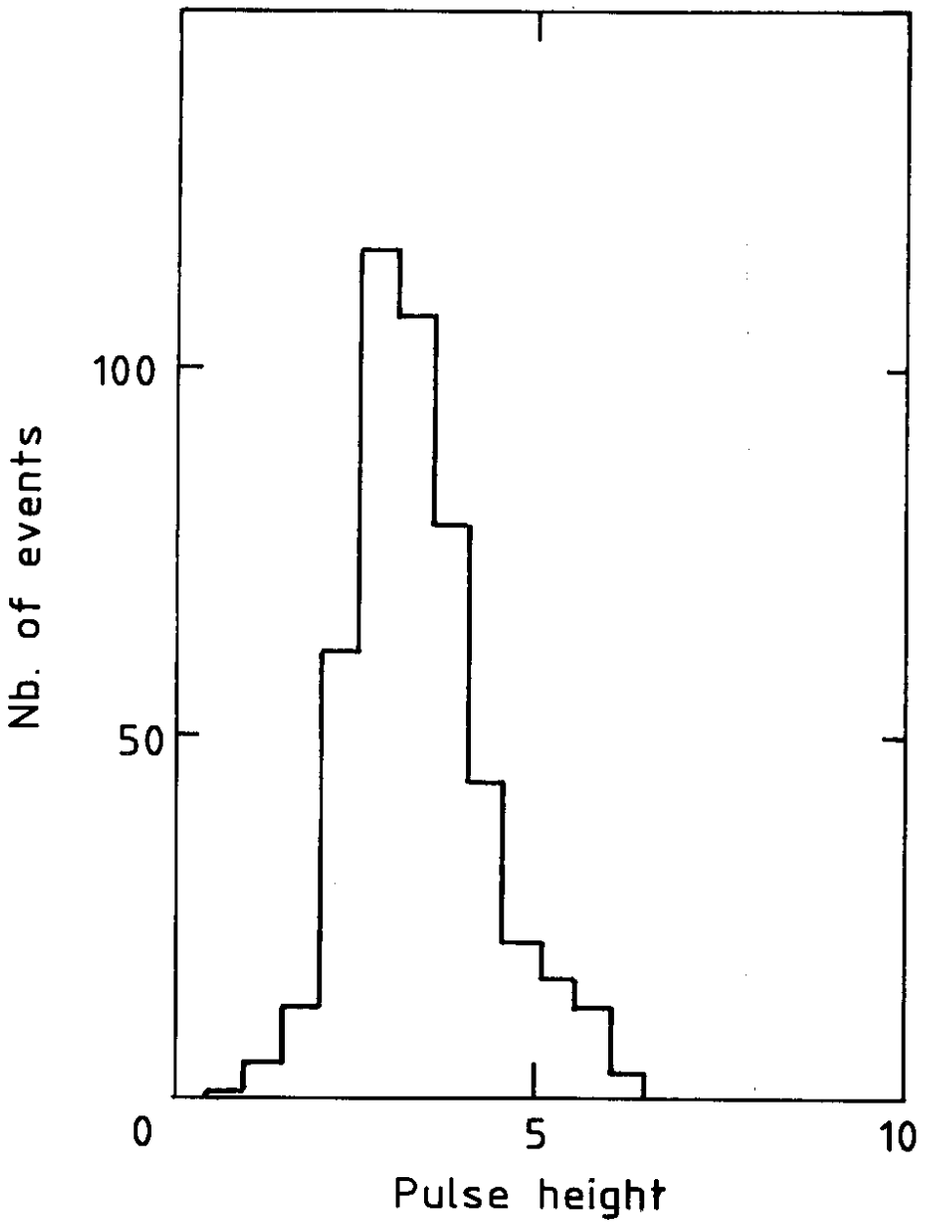

Figure 6

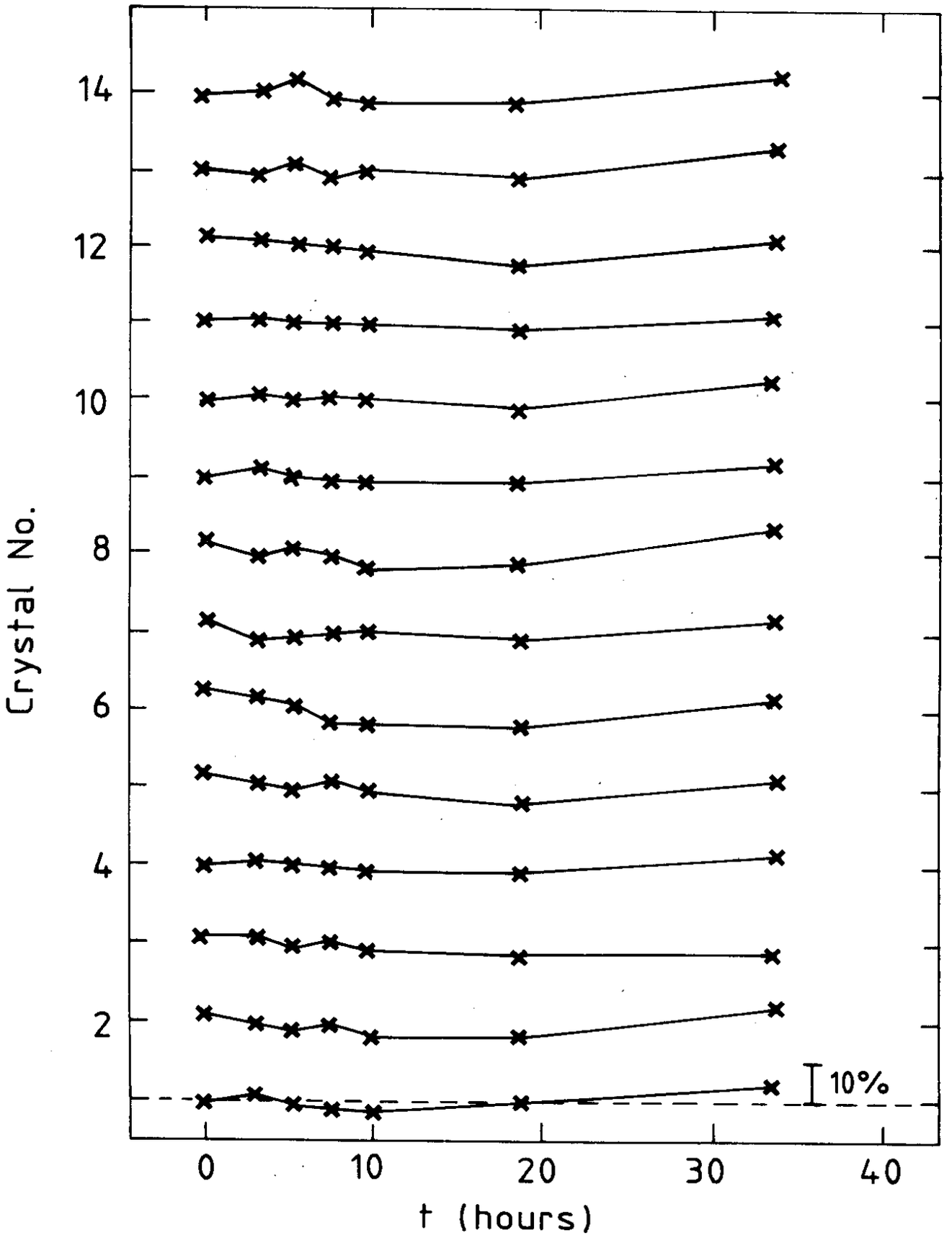

Figure 7

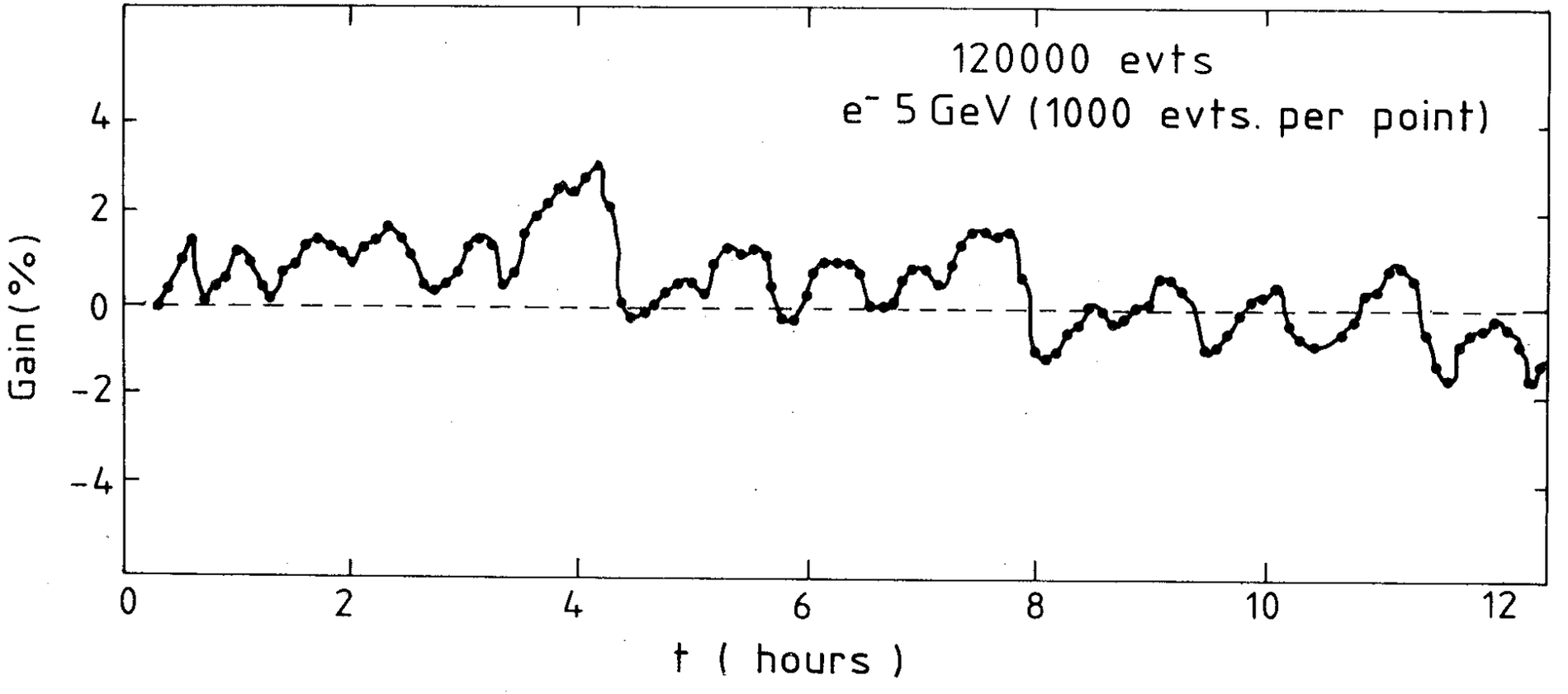
120000 evts
e⁻ 5 GeV (1000 evts. per point)
Gain (%)
4
2
0
-2
-4
0
2
4
6
8
10
12
t (hours)

Figure 8

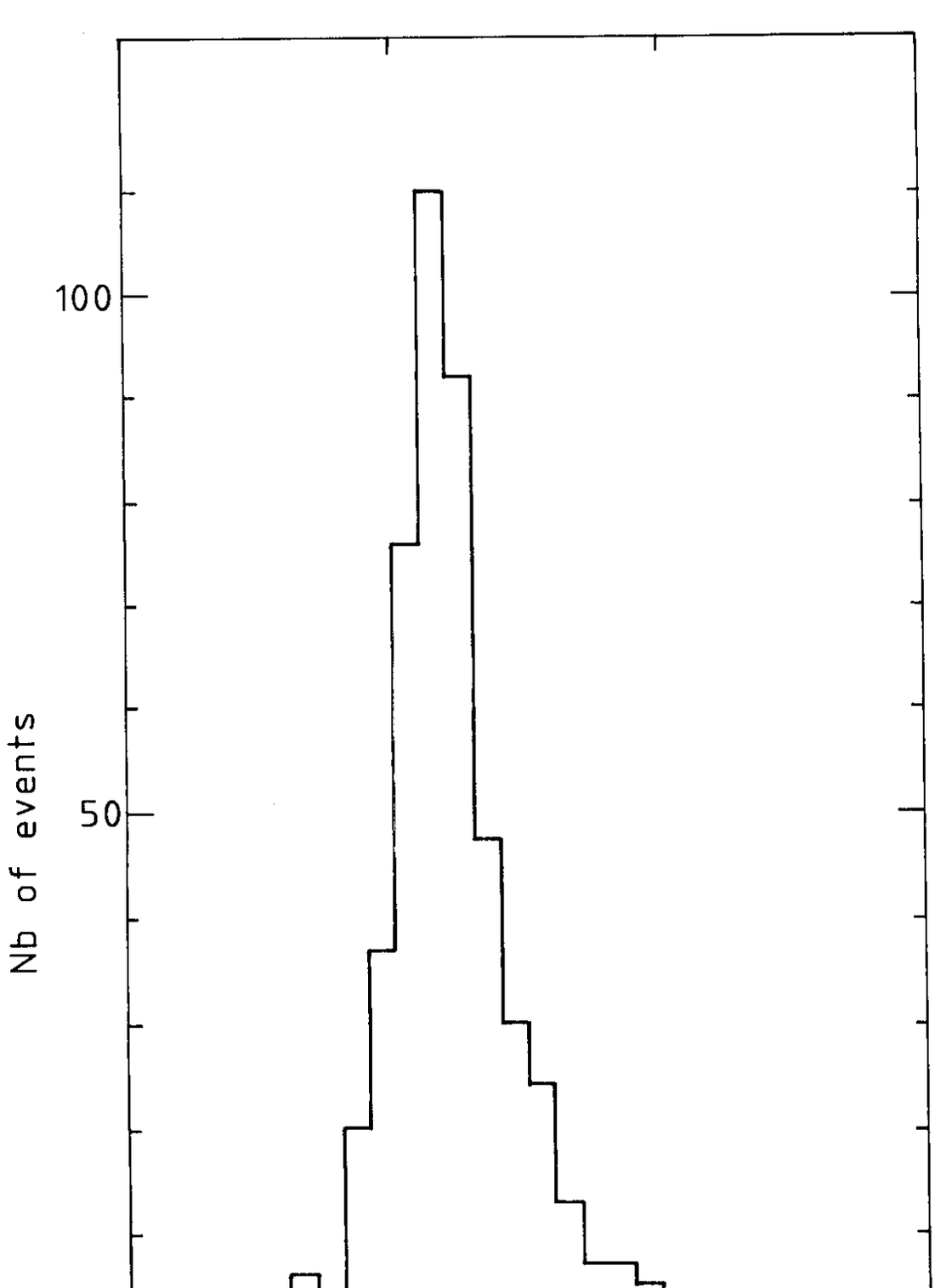

Figure 9

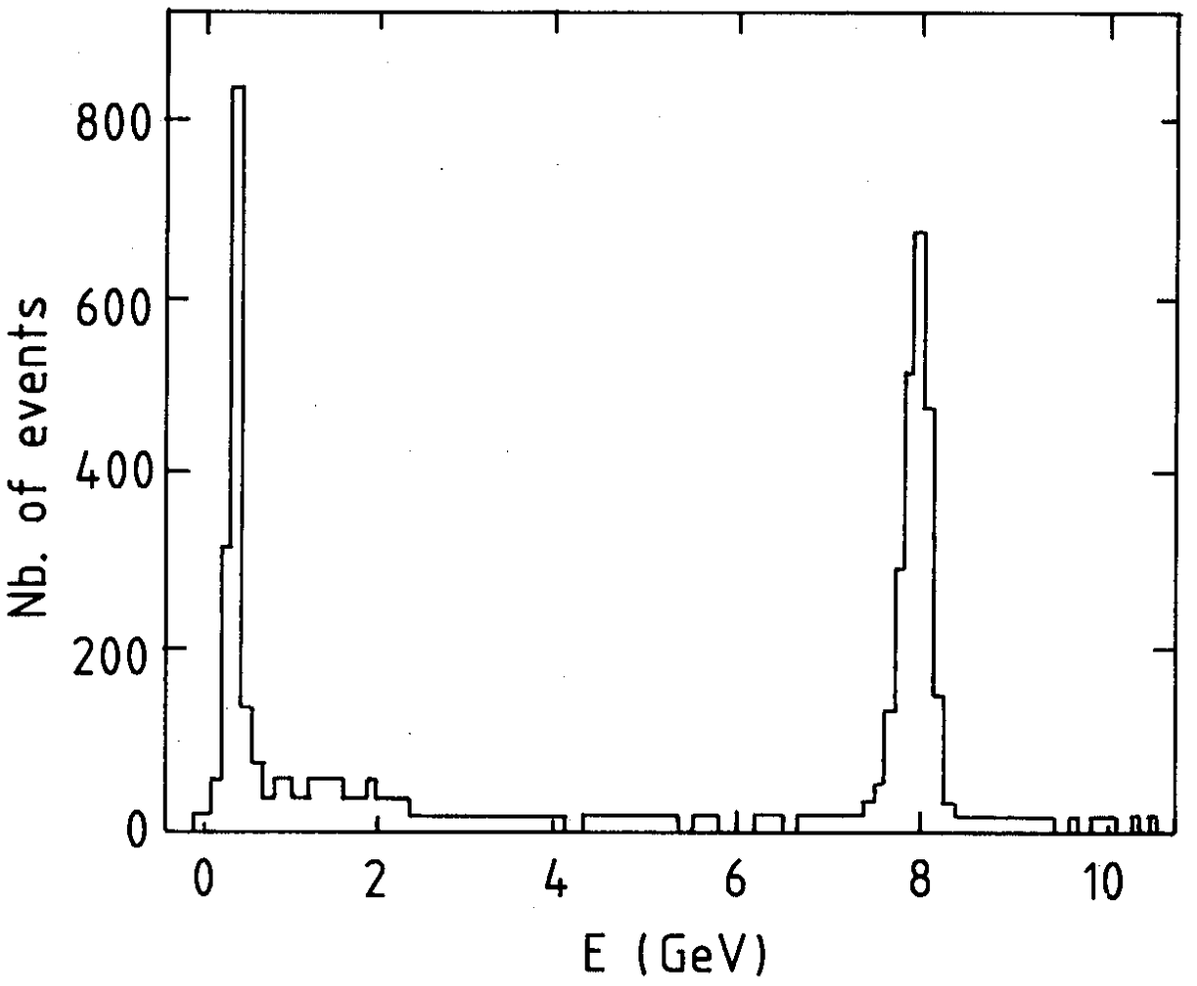

Figure 10

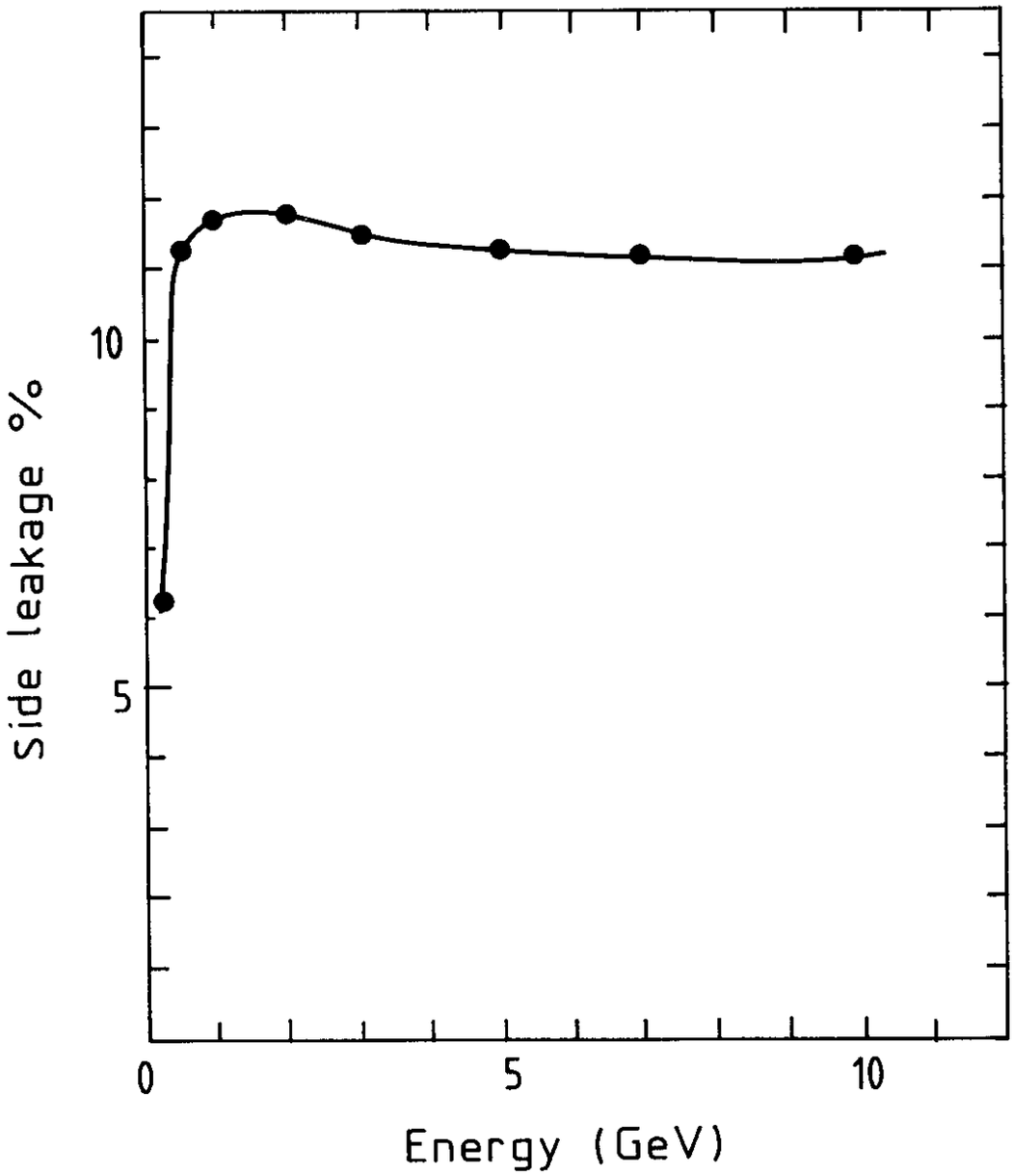

Figure 11

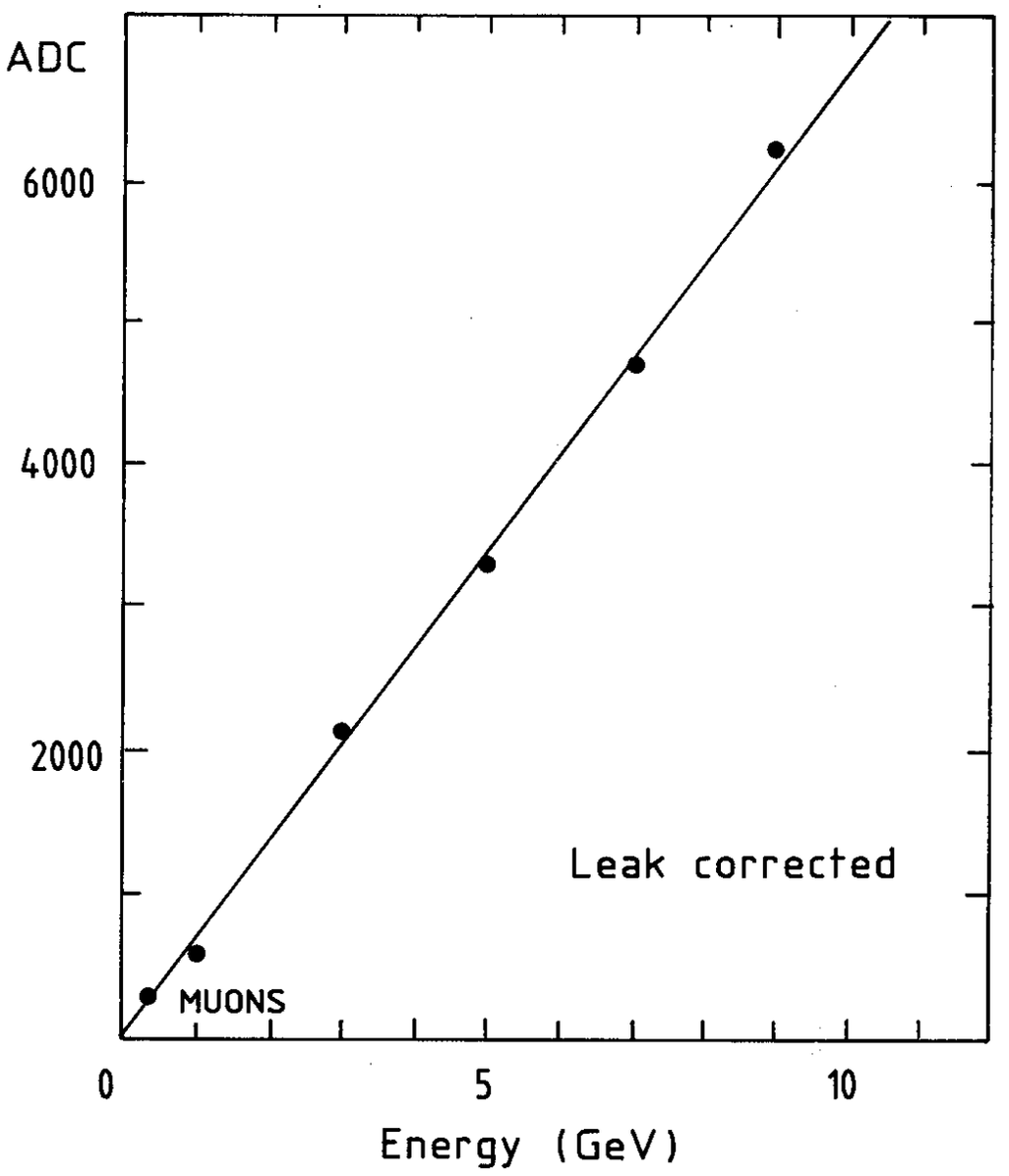

Figure 12

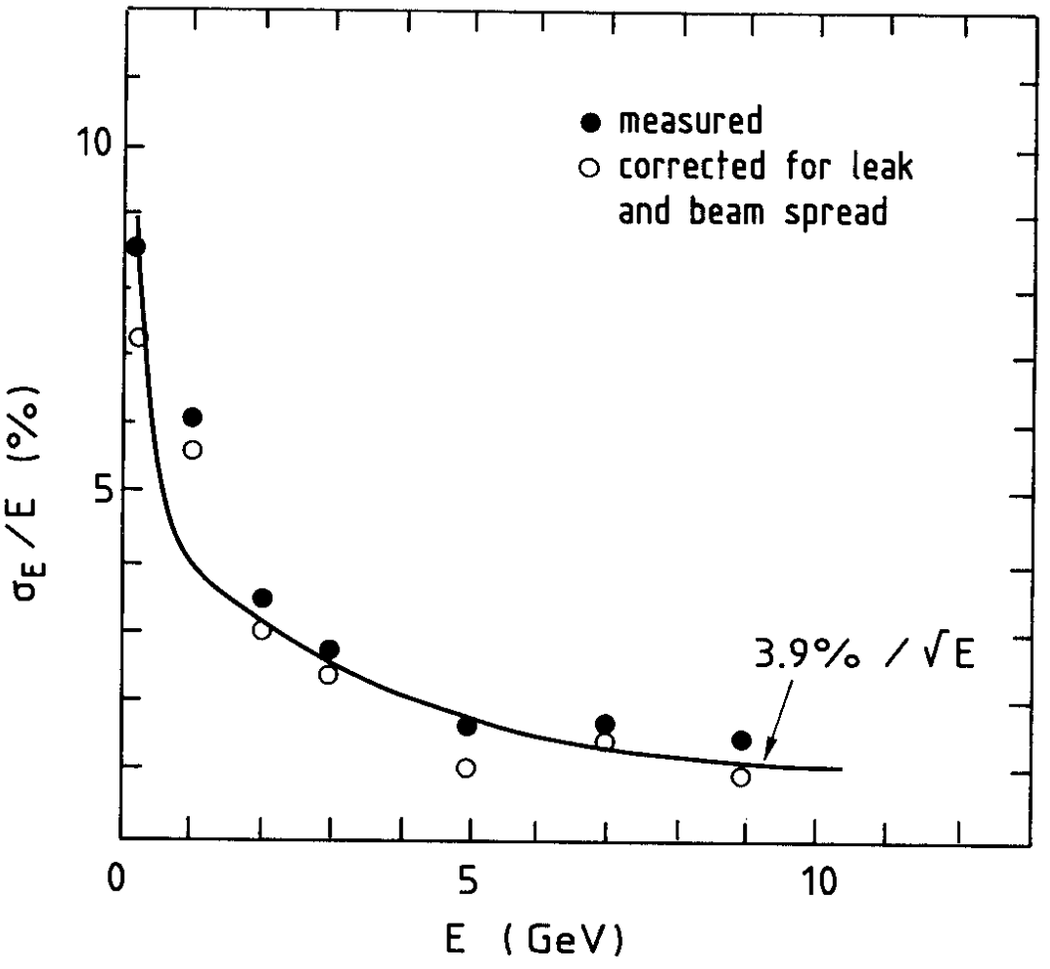
measured
corrected for leak
and beam spread
3.9% / √E
10
5
0
5
10
σE / E (%)
E (GeV)

Figure 13

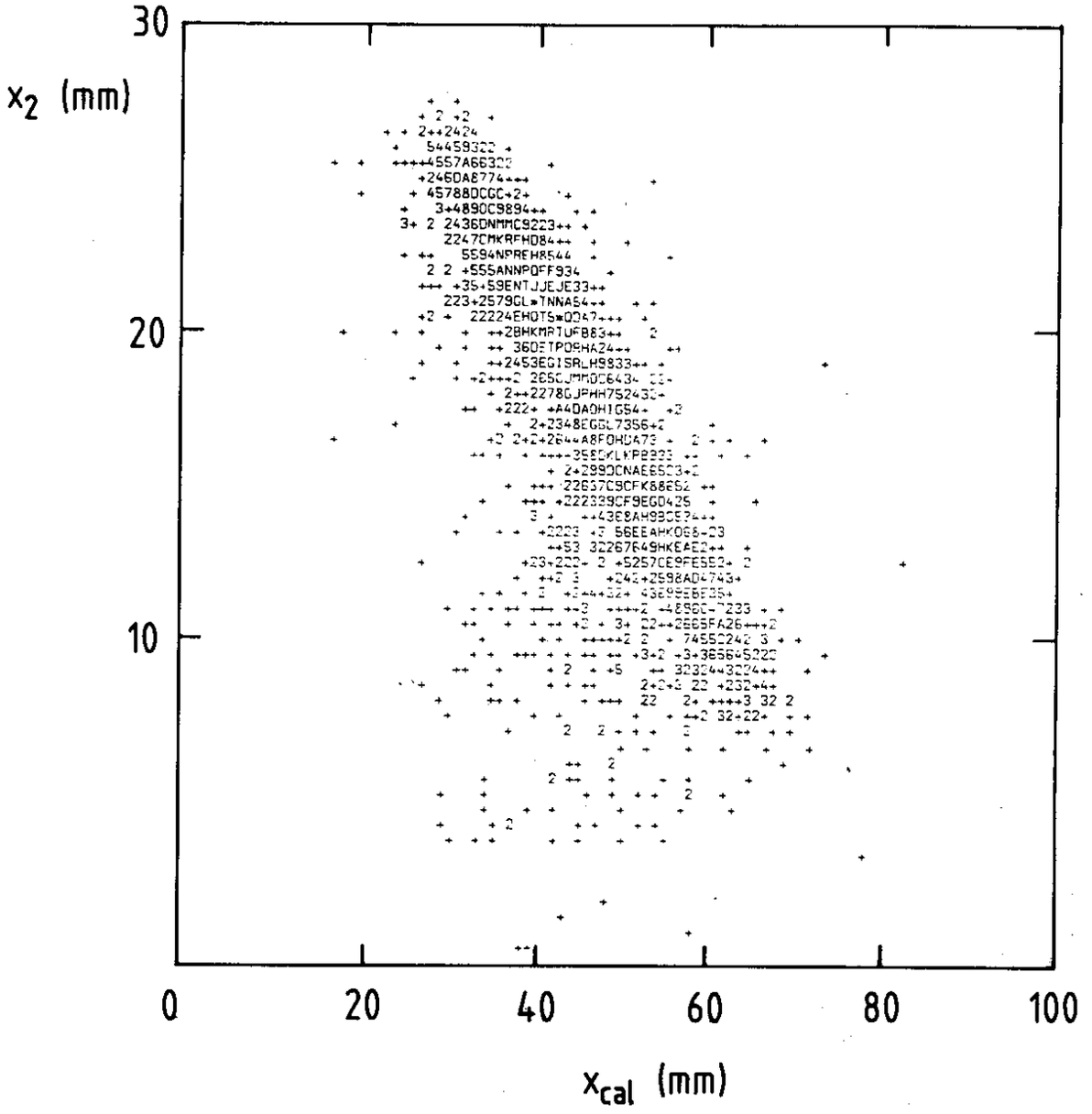

Figure 14

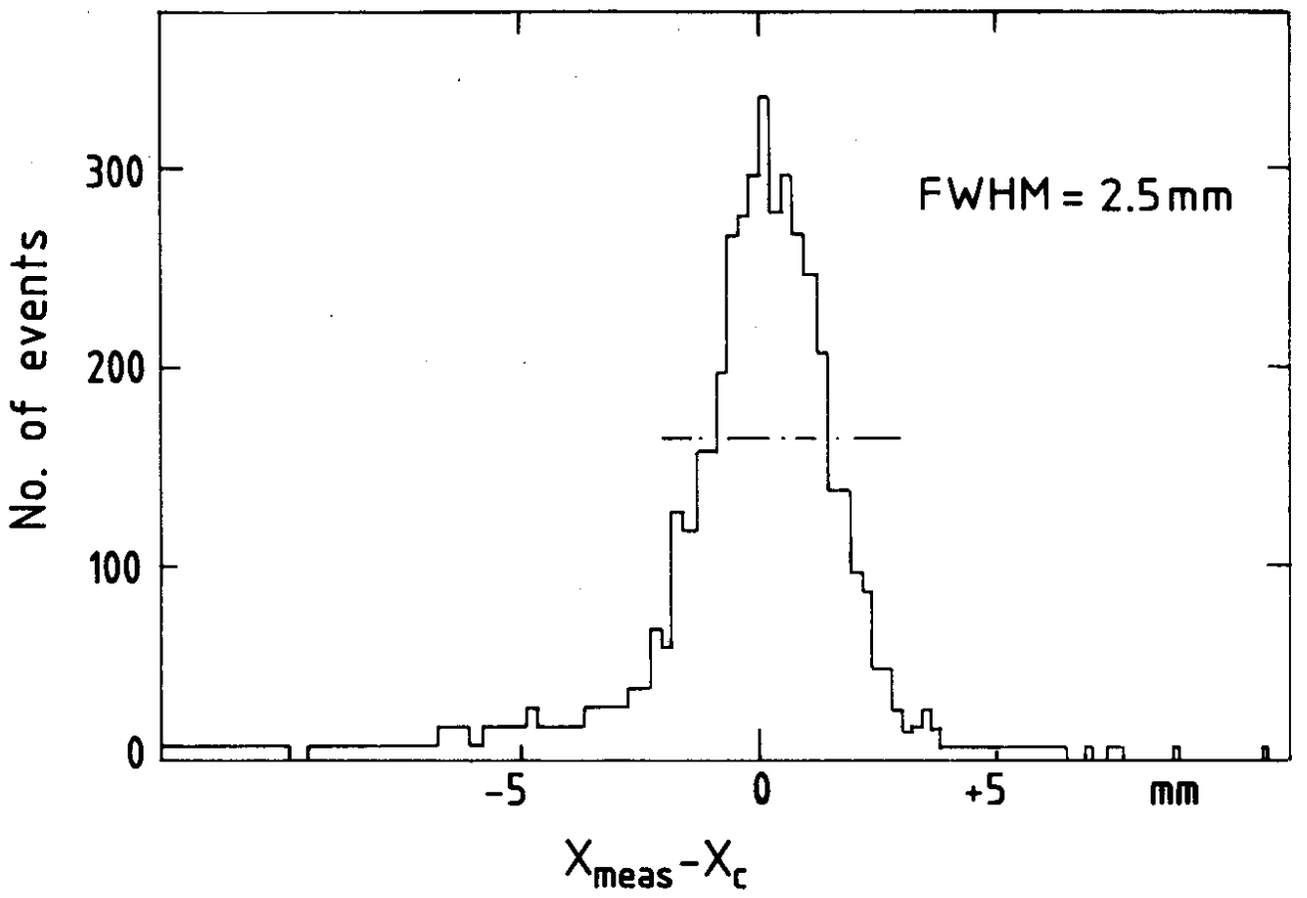

Figure 15

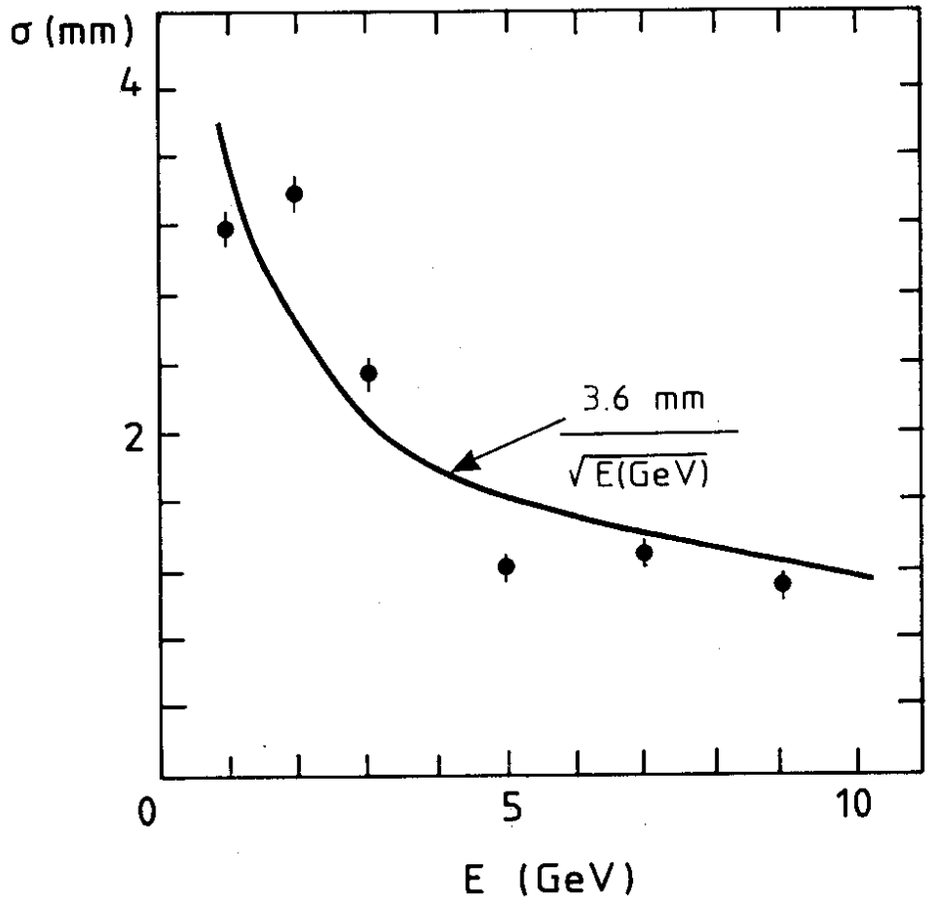

Figure 16

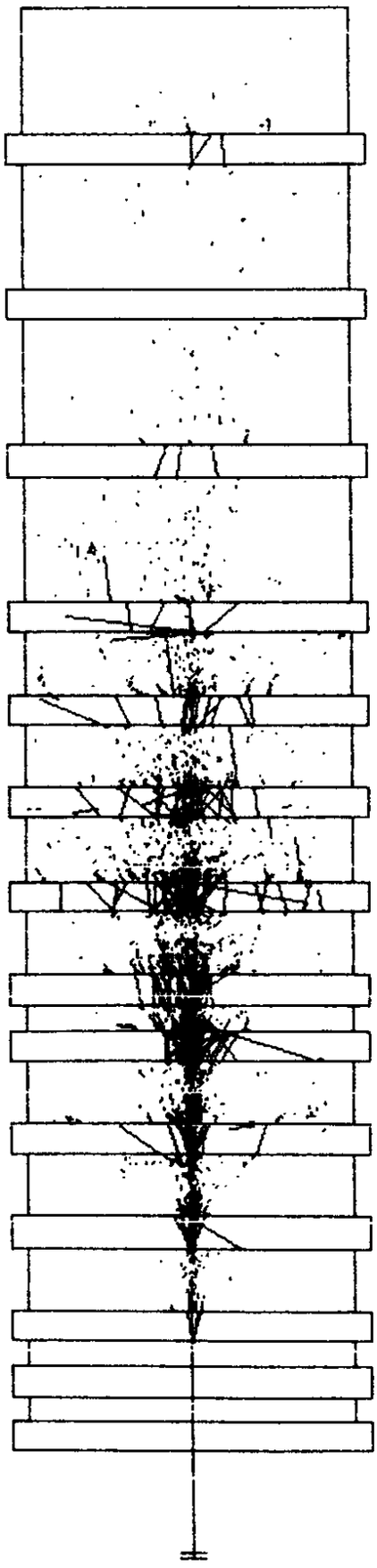

Figure 17

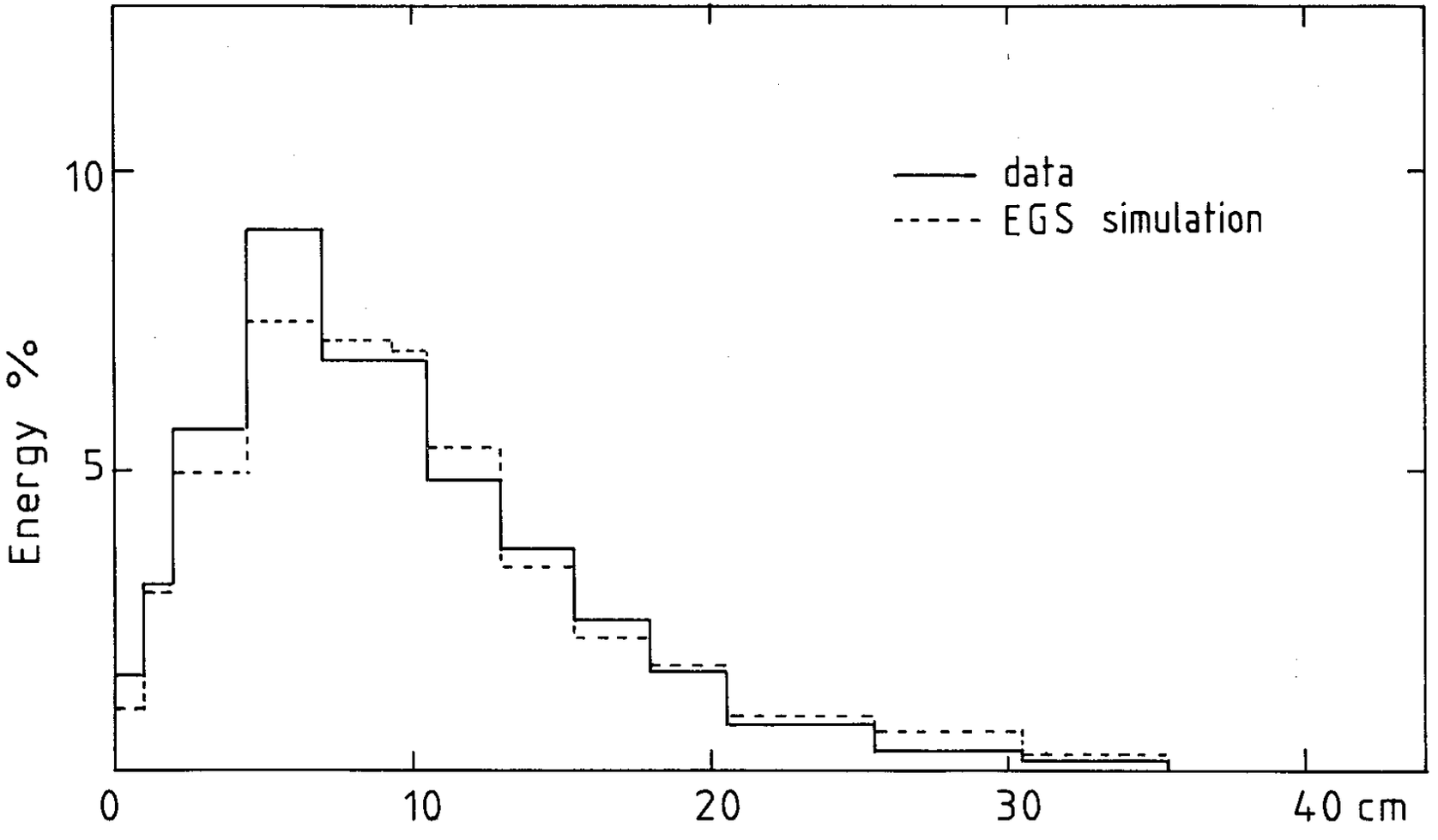

Figure 18a

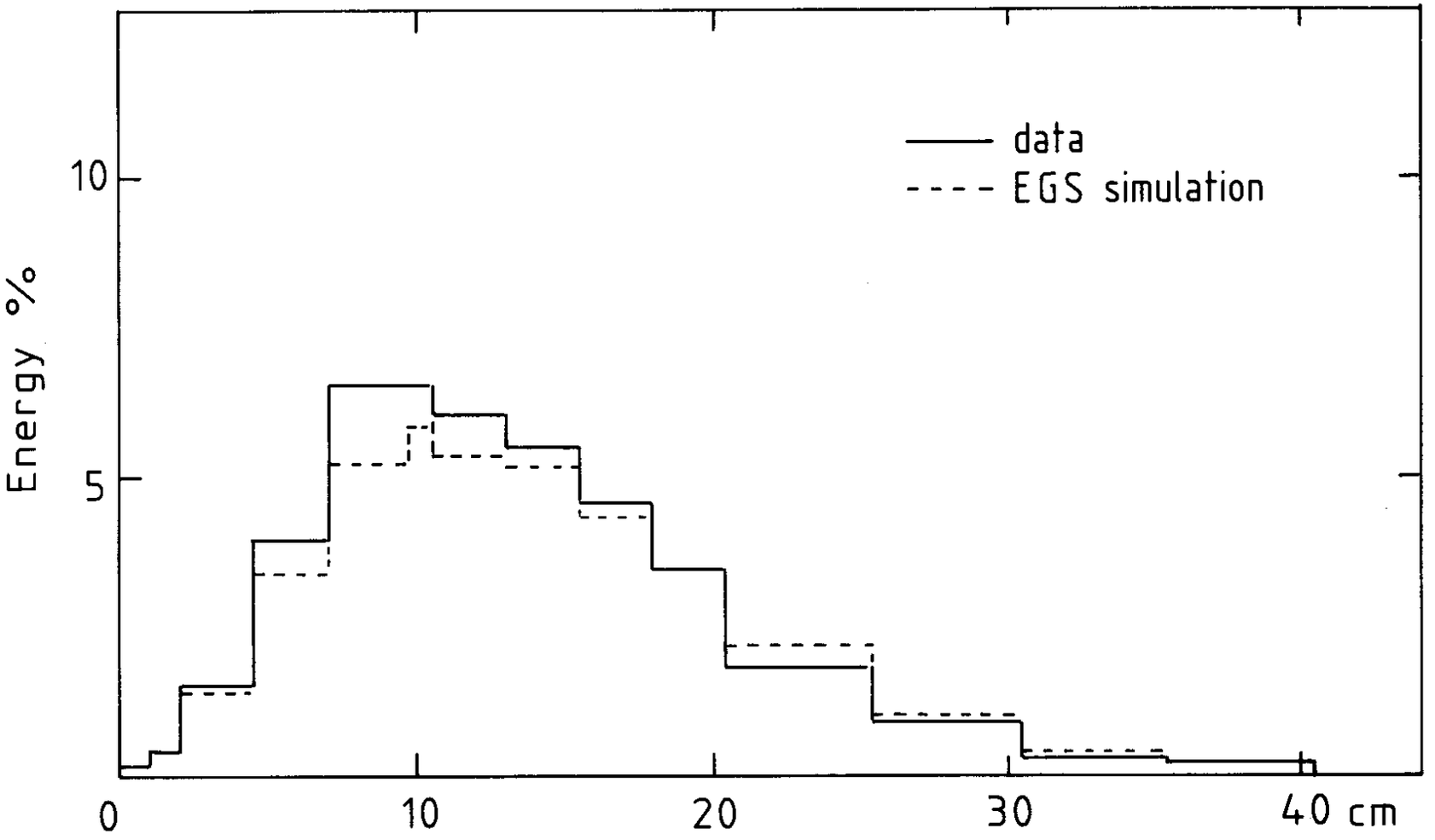

Figure 18b

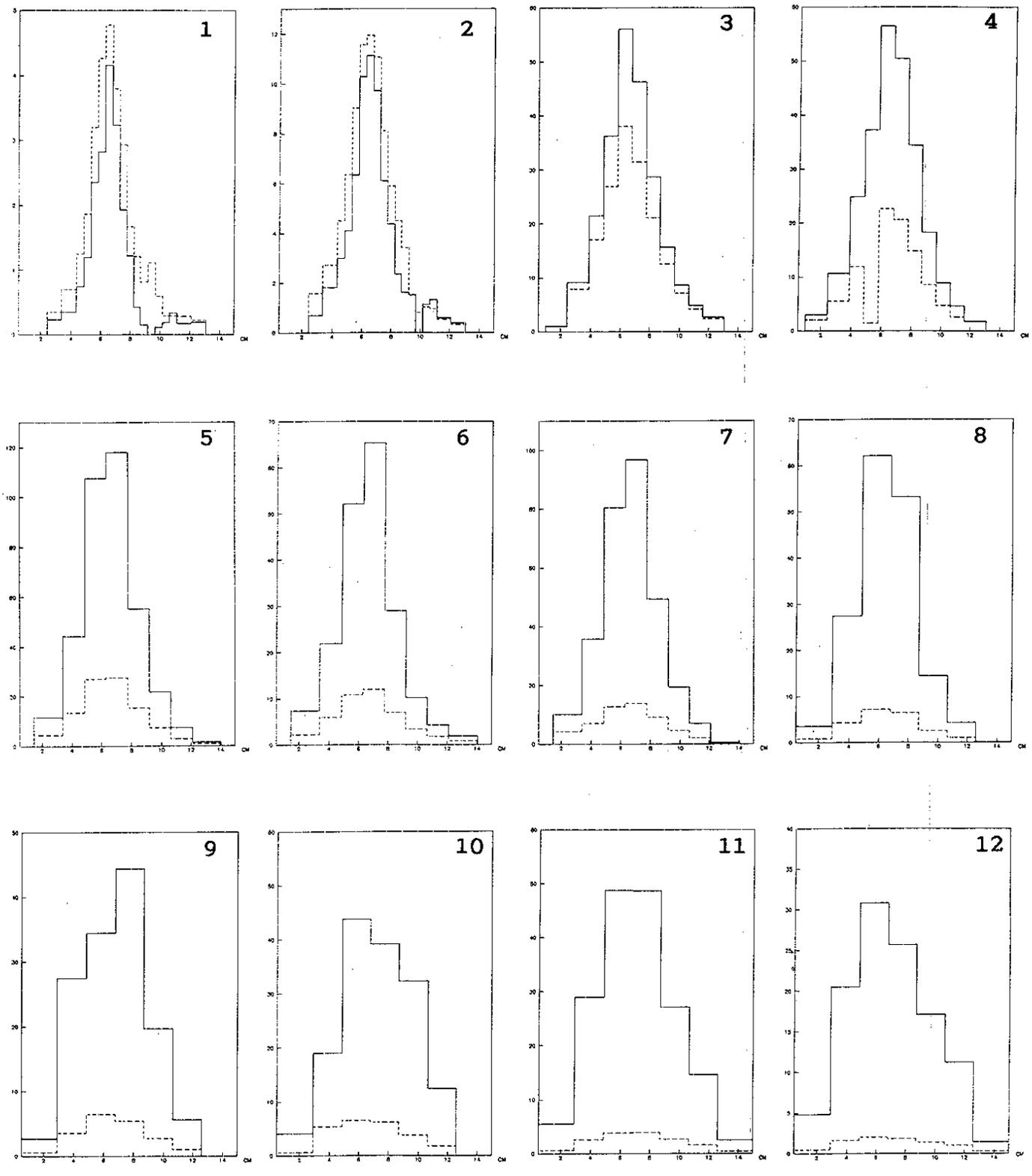

Figure 19

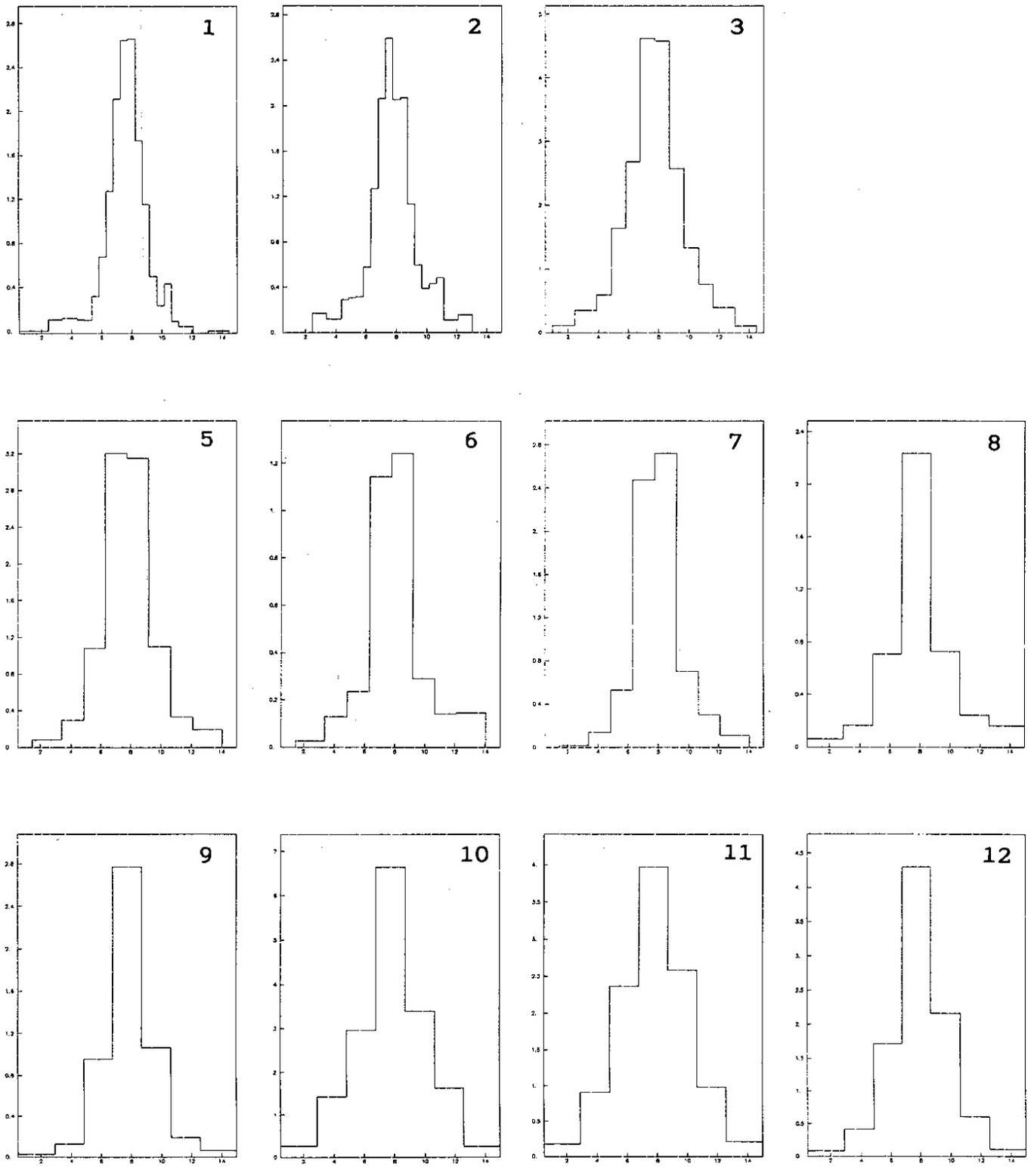

Figure 20

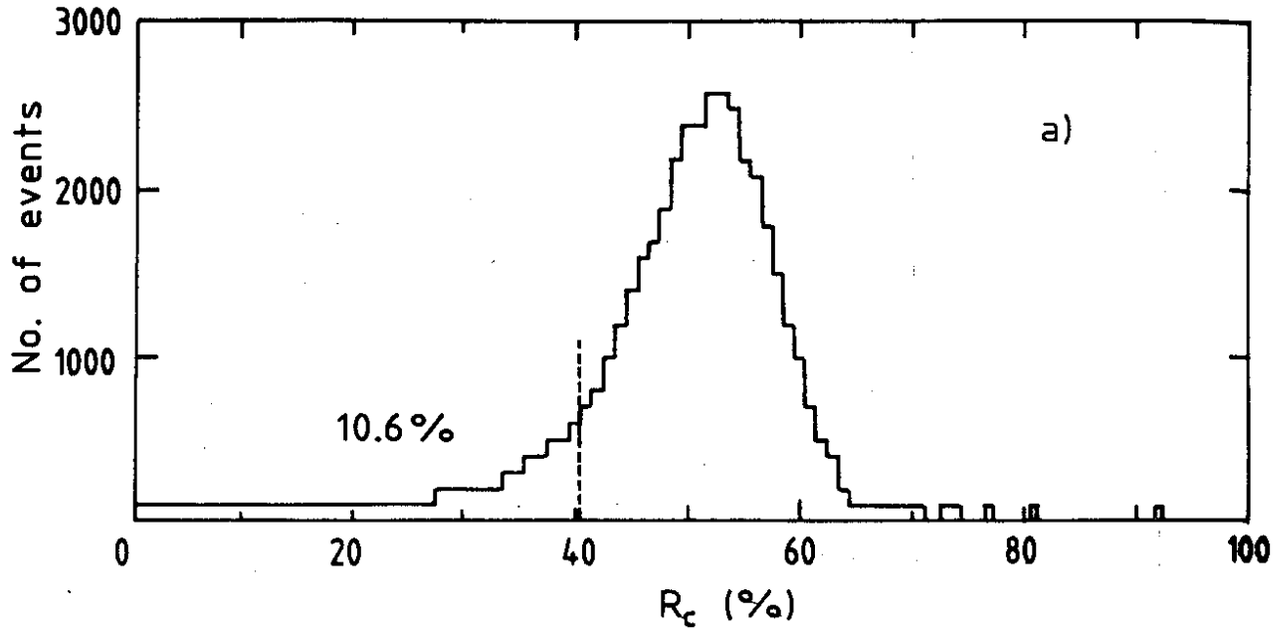
3000
2000
1000
No. of events
a)
10.6 %
0
20
40
60
80
100
R_c (%)

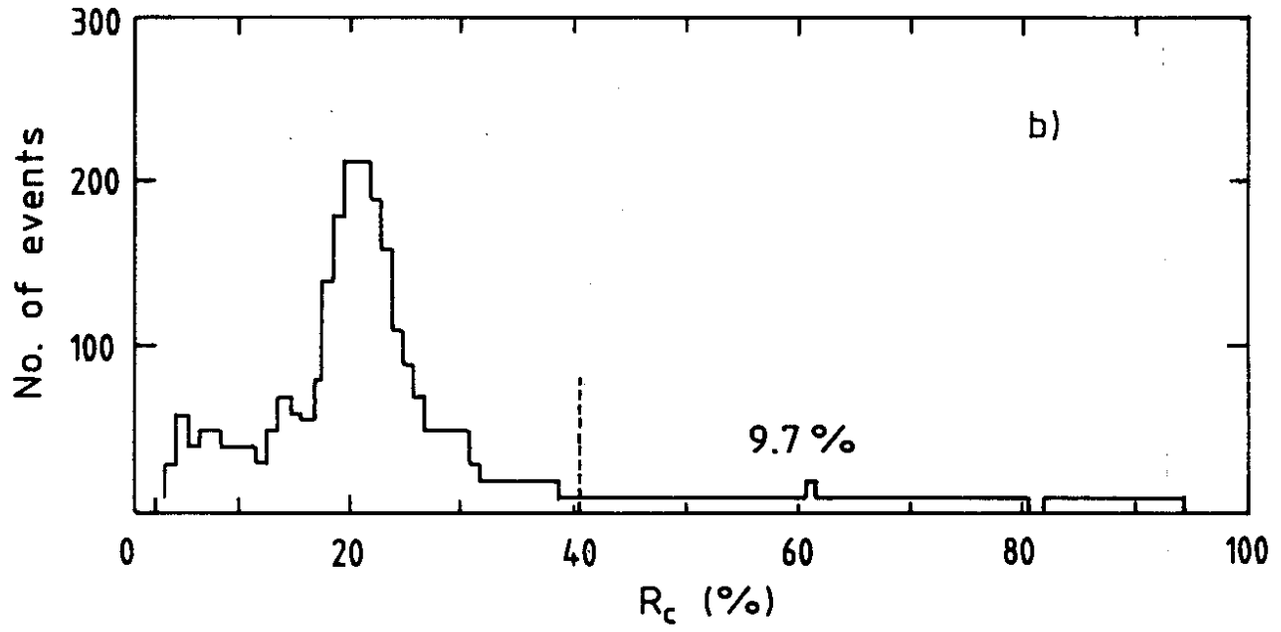
300
200
100
No. of events
b)
9.7 %
0
20
40
60
80
100
R_c (%)

Figure 21

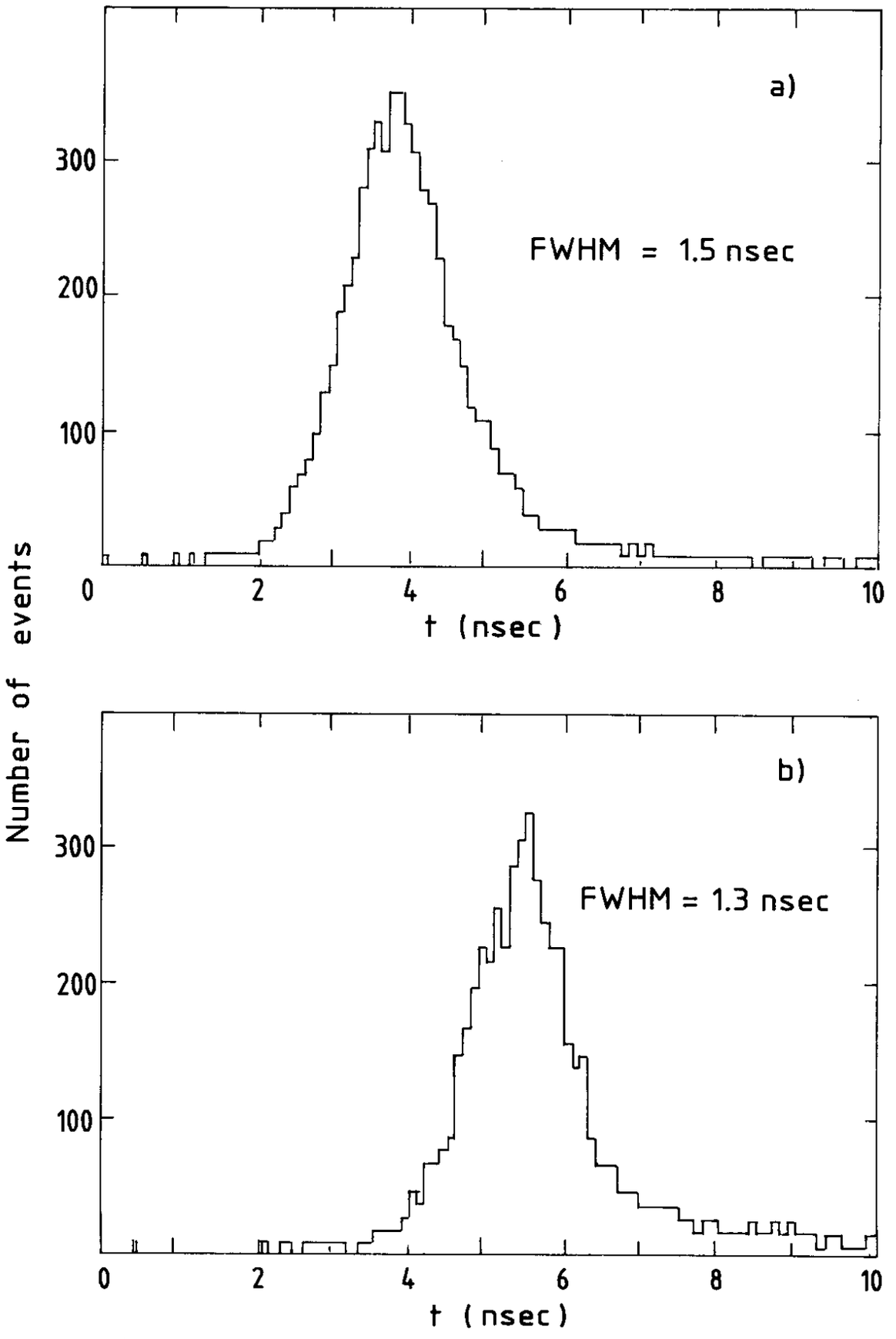
a)
FWHM = 1.5 nsec
300
200
100
0
2
4
6
8
10
t (nsec)
Number of events
b)
FWHM = 1.3 nsec
300
200
100
0
2
4
6
8
10
t (nsec)

Figure 22

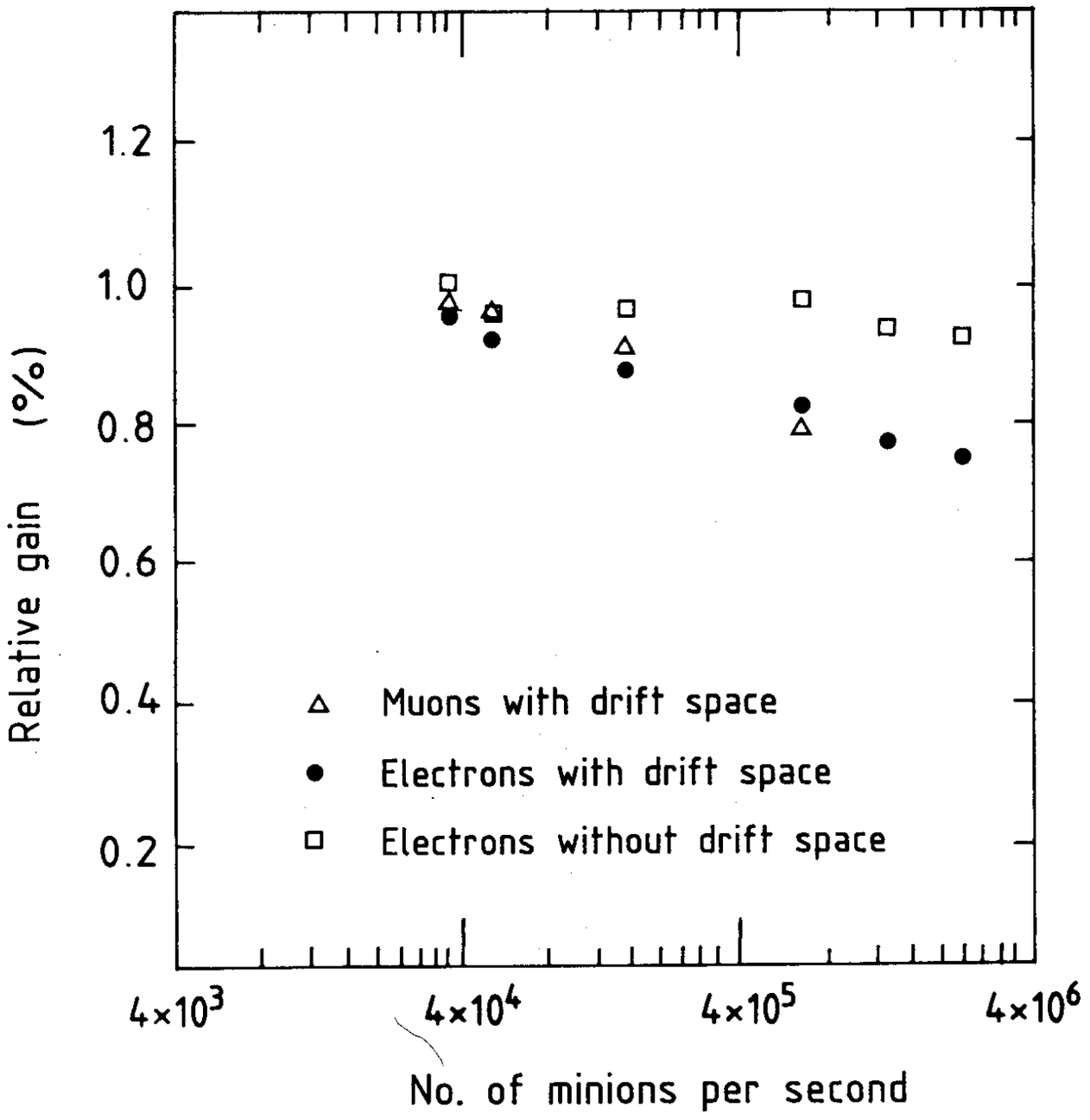
1.2
1.0
0.8
0.6
0.4
0.2
Relative gain (%)
Muons with drift space
Electrons with drift space
Electrons without drift space
4×10³
4×10⁴
4×10⁵
4×10⁶
No. of minions per second

Figure 23

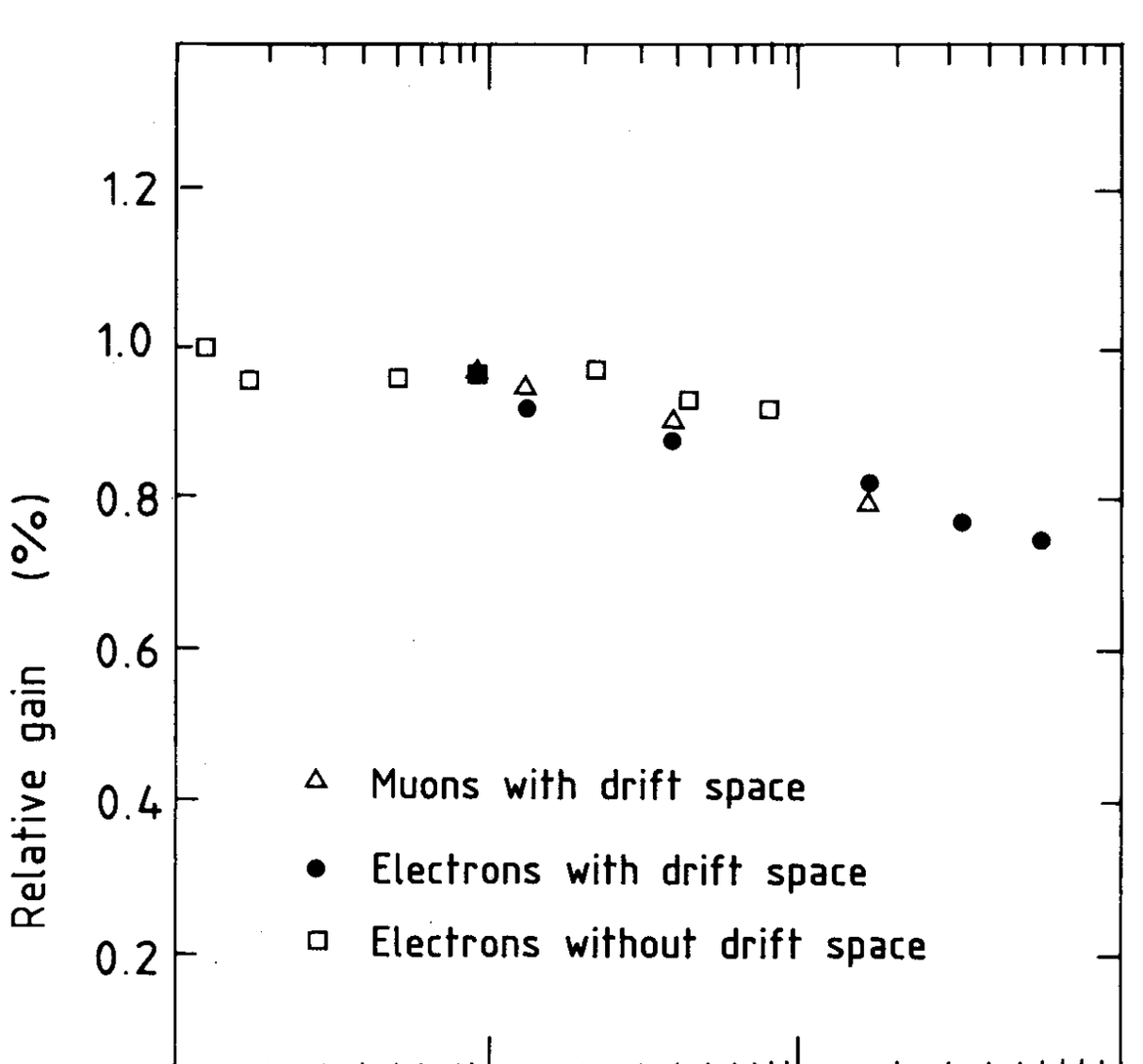
1.2
1.0
0.8
0.6
0.4
0.2
Relative gain (%)
Muons with drift space
Electrons with drift space
Electrons without drift space
10^{-12}
10^{-11}
10^{-10}
10^{-9}
Intensity (A/mm of wire)

Figure 24